Article

Developmental Cell

GCNA Interacts with Spartan and Topoisomerase II to Regulate Genome Stability

Graphical Abstract

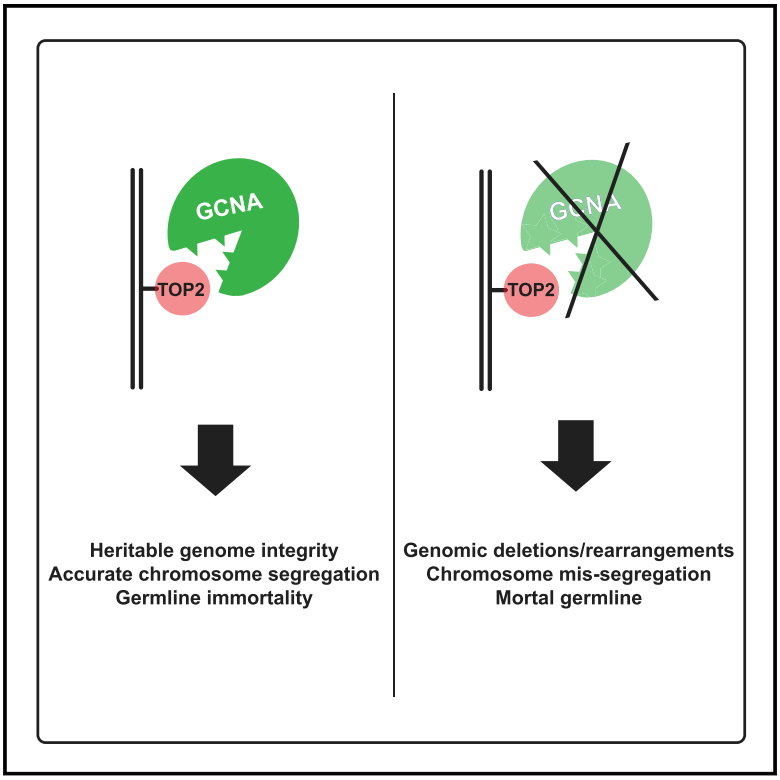

Highlights

- *gcna-1* is essential for germline immortality and integrity of the heritable genome
- GCNA works in tandem with Spartan (DVC-1) to maintain genomic integrity
- GCNA promotes the resolution of TOP2 DPCs in the germline and early embryo in worms and mice

Authors

Gregoriy A. Dokshin, Gregory M. Davis, Ashley D. Sawle, ..., David C. Page, Craig C. Mello, Michelle A. Carmell

Correspondence

craig.mello@umassmed.edu (C.C.M.), mcarmell@wellesley.edu (M.A.C.)

In Brief

DNA topoisomerases help unwind DNA but occasionally get trapped, resulting in DNA-protein crosslinks (DPCs). DPCs damage DNA and threaten genomic integrity. Dokshin et al. find that GCNA protein family complements standard DPC processing machinery in resolving topoisomerase II DPCs to ensure heritable genome stability and germline immortality.

Dokshin et al., 2020, Developmental Cell *52*, 53–68
January 6, 2020
https://doi.org/10.1016/j.devcel.2019.11.006

CellPress

Developmental Cell
Article

GCNA Interacts with Spartan and Topoisomerase II to Regulate Genome Stability

Gregoriy A. Dokshin,[1,11] Gregory M. Davis,[2,11] Ashley D. Sawle,[3] Matthew D. Eldridge,[3] Peter K. Nicholls,[4] Taylin E. Gourley,[2] Katherine A. Romer,[4,5] Luke W. Molesworth,[2] Hannah R. Tatnell,[2] Ahmet R. Ozturk,[1] Dirk G. de Rooij,[4,6,7] Gregory J. Hannon,[3,8] David C. Page,[4,9] Craig C. Mello,[1,10,12,*] and Michelle A. Carmell[1,4,8,*]
[1]RNA Therapeutics Institute, University of Massachusetts Medical School, Worcester, MA 01605, USA
[2]School of Health and Life Sciences, Federation University, VIC 3841, Australia
[3]Cancer Research UK Cambridge Institute, University of Cambridge, Cambridge CB2 0RE, UK
[4]Whitehead Institute, 455 Main Street, Cambridge, MA 02142, USA
[5]Computational and Systems Biology Program, Massachusetts Institute of Technology, Cambridge, MA 02142, USA
[6]Reproductive Biology Group, Division of Developmental Biology, Department of Biology, Faculty of Science, Utrecht University, Utrecht 3584, the Netherlands
[7]Center for Reproductive Medicine, Academic Medical Center, University of Amsterdam 1105, the Netherlands
[8]Cold Spring Harbor Laboratory, Cold Spring Harbor, NY 11724, USA
[9]Howard Hughes Medical Institute, Whitehead Institute, Cambridge, MA 02142, USA
[10]Howard Hughes Medical Institute, University of Massachusetts Medical School, Worcester, MA 01605, USA
[11]These authors contributed equally
[12]Lead Contact
*Correspondence: craig.mello@umassmed.edu (C.C.M.), mcarmell@wellesley.edu (M.A.C.)
https://doi.org/10.1016/j.devcel.2019.11.006

SUMMARY

GCNA proteins are expressed across eukarya in pluripotent cells and have conserved functions in fertility. GCNA homologs Spartan (DVC-1) and Wss1 resolve DNA-protein crosslinks (DPCs), including Topoisomerase-DNA adducts, during DNA replication. Here, we show that GCNA mutants in mouse and *C. elegans* display defects in genome maintenance including DNA damage, aberrant chromosome condensation, and crossover defects in mouse spermatocytes and spontaneous genomic rearrangements in *C. elegans*. We show that GCNA and topoisomerase II (TOP2) physically interact in both mice and worms and colocalize on condensed chromosomes during mitosis in *C. elegans* embryos. Moreover, *C. elegans gcna-1* mutants are hypersensitive to TOP2 poison. Together, our findings support a model in which GCNA provides genome maintenance functions in the germline and may do so, in part, by promoting the resolution of TOP2 DPCs.

INTRODUCTION

DNA in all living systems is exposed to damage from both endogenous and exogenous sources. Resulting mutations in pluripotent cells can cause premature aging, cancer, and developmental defects. Mutations in germ cells are acutely harmful as these cells are uniquely tasked with passing their genomes to the next generation, a process critical for both short-term reproductive success and long-term fitness and survival of all species. Germ cells cope with insults that somatic cells never encounter—hundreds of meiotic double-strand breaks, homologous recombination, massive exchange of histones, and dramatic chromosome condensation. As such, specialized pathways have evolved to protect the genomic integrity of pluripotent cells and germ cells (Cerutti and Casas-Mollano, 2006; Juliano et al., 2010, 2011; Shabalina and Koonin, 2008; van Wolfswinkel, 2014).

We previously discovered the GCNA protein family that is present across eukarya in cells carrying a heritable genome, including pluripotent cells and germ cells of diverse multicellular animals. *Gcna* mutations in both *C. elegans* and mice significantly impact reproduction, suggesting that GCNA has functioned in the germline for at least 600 million years (Carmell et al., 2016). GCNA proteins belong to a larger family that includes Spartan (SPRTN [DVC-1]) and Wss1, which function in DNA-protein crosslink (DPC) repair and eliminate proteins that are inappropriately crosslinked to DNA (Barker et al., 2005; Carmell et al., 2016; Fielden et al., 2018). Endogenous reactive aldehydes, ionizing radiation, ultraviolet (UV) light, chemotherapeutics, chemical crosslinkers, and trapped enzymatic intermediates all cause DNA-protein crosslinks (Stingele et al., 2015). DPCs interfere with transcription, unwinding, replication, and repair of DNA (Nakano et al., 2012, 2013; Yudkina et al., 2018). The SprT domains of Spartan and Wss1 proteolyze DPCs to make way for downstream repair (Balakirev et al., 2015; Ghosal et al., 2012; Maskey et al., 2017; Stingele et al., 2016, 2014). Aside from their role in proteolysis, Spartan and Wss1 also support translesion synthesis (TLS) by recruiting the segregase VCP (p97) and bind PCNA and ubiquitin (for Spartan), and SUMO (for Wss1) at stalled replication forks during S phase (Stingele et al., 2017).

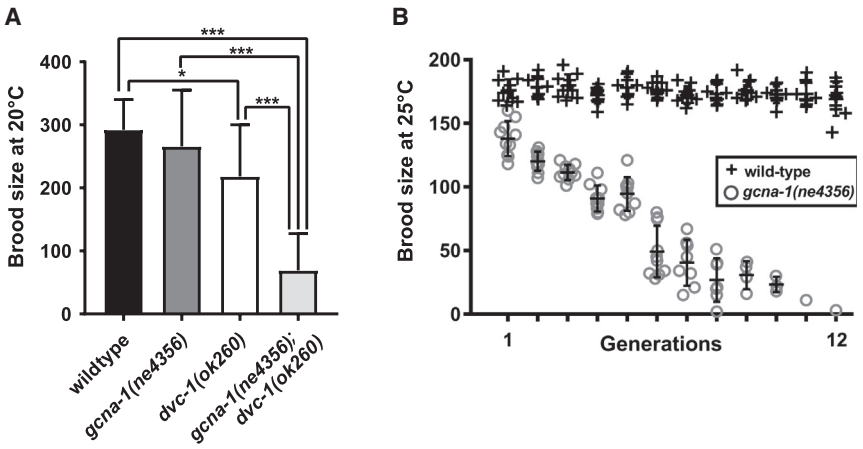

Figure 1. *gcna-1* Mutants Exhibit a Distinct Germline Phenotype Associated with Genomic Decline

(A) Brood size comparison between wild type, *gcna-1(ne4356), dvc-1(ok260)*, and *gcna-1(ne4356);dvc-1(ok260)* double mutants (Error bars, SDM. ***p < 0.0001, *p < 0.05).

(B) Brood sizes across twelve generations. Each symbol represents the number of progeny derived from a single hermaphrodite. p < 0.0001 at all generations. (Error bars, SDM.) See also Figure S1.

Topoisomerases are crucial targets of Spartan and Wss1 (Lopez-Mosqueda et al., 2016; Stingele et al., 2014; Vaz et al., 2016). Topoisomerases modify DNA topology and are necessary for DNA replication, transcription, recombination, and chromosome condensation and segregation (Wang, 1996). TOP1 and TOP2 make single and double-stranded DNA breaks, respectively, to resolve helical torsion, knots, and catenanes. Their catalytic mechanisms have covalent reaction intermediates in which a tyrosine is crosslinked to DNA; abortive reaction events leave behind DPCs (Champoux, 2001; Deweese and Osheroff, 2009; Wang, 2002).

Spartan is a constitutive component of the replisome during S phase and resolves DPCs blocking replication forks (Ghosal et al., 2012; Mórocz et al., 2017; Vaz et al., 2016). DPCs are also generated when Spartan is absent due to degradation by APC-Cdh1 (Mosbech et al., 2012). TOP2 DPCs are abundant outside of S phase, as it is highly expressed during G2 and M phases, when it is necessary for chromatin condensation and proper separation of sister chromatids (DiNardo et al., 1984; Li et al., 2013; Maeshima and Laemmli, 2003; Uemura et al., 1987; Uemura and Tanagida, 1986; Woessner et al., 1991).

GCNA and TOP2 are both abundant in the germline of diverse organisms. TOP2 has germline-specific functions including separation of recombined chromosomes, crossover interference, histone exchange, and sperm chromatin condensation (Akematsu et al., 2017; Hartsuiker et al., 1998; Hughes and Hawley, 2014; Jaramillo-Lambert et al., 2016; Leduc et al., 2008; Marchetti et al., 2001; Marcon and Boissonneault, 2004; Mengoli et al., 2014; Rathke et al., 2007; Tateno and Kamiguchi, 2001). Accordingly, topoisomerase dysfunction during meiosis in a wide array of organisms including yeasts, mammals, fly, and worm causes chromosome segregation defects that result in aneuploidy and chromosome breakage in spores and gametes (Hartsuiker et al., 1998; Hughes and Hawley, 2014; Jaramillo-Lambert et al., 2016; Marchetti et al., 2001). TOP2 also functions in the early embryo where it is necessary for paternal chromatin remodeling and activation of the zygotic genome after fertilization (Tang et al., 2017; Wong et al., 2018). In addition to TOP2, germ cells also express a specialized topoisomerase, SPO11. SPO11 creates meiotic double-strand breaks and facilitates sperm chromatin condensation and, as a part of its normal function, remains covalently attached to DNA ends (Akematsu et al., 2017; Keeney et al., 1997). Taken together, early embryo and germline genomes are expected to carry an extra burden of topoisomerase DPCs relative to somatic cells.

Here, we show that in the absence of GCNA-1, the genome is subject to mutations that cause deterioration of the genome over successive generations. This phenotype is consistent with that of *dvc-1*, and is genetically enhanced in double mutants with *dvc-1* suggesting a parallel role for GCNA-1 and DVC-1 in DPC repair. Our data point toward a role for GCNA in supporting processing of TOP2 DPCs. We show that *C. elegans* GCNA-1 and TOP-2 physically interact and colocalize during mitosis and that *gcna-1* mutants are sensitive to TOP2 poison. Mouse GCNA also interacts with TOP2, and *Gcna*-mutant mice exhibit abnormalities consistent with the inability to process DPCs. Together, our findings support the model that GCNA promotes the resolution of TOP2 DPCs in the germline and early embryo.

RESULTS

gcna-1 Mutants Exhibit a Distinct Germline Phenotype Associated with Genomic Decline

GCNA, Spartan, and Wss1 share highly homologous SprT protease domains and large, rapidly evolving disordered regions containing motifs for binding ubiquitin or SUMO (Carmell et al., 2016). To investigate whether GCNA, Spartan, and Wss1 have similar functions, we characterized the phenotype of *C. elegans gcna-1* mutants. Like most animals, in addition to *gcna-1, C. elegans* has a single related gene that is most similar to Spartan (*dvc-1*). While both *gcna-1* and *dvc-1* mutant *C. elegans* display decreased brood sizes under some conditions, only *dvc-1* broods are markedly smaller than wild type at 20°C (Figure 1A) (Carmell et al., 2016; Mosbech et al., 2012). To determine if *gcna-1* mutants display germline morphological defects, we examined animals carrying *gcna-1(ne4356)*, a 1,748-bp deletion that removes the start codon. *gcna-1(ne4356)* mutants were stained with the mitotic proliferative marker, phospho-histone 3 (PH3), and with PGL-1, a marker of P-granules that serve as hubs of post-transcriptional germline control (Brangwynne et al., 2009; Hendzel et al., 1997; Voronina, 2013). We observed wild-type distributions of both markers (Figures S1A and S1B), suggesting that the germlines of *gcna-1(ne4356)* mutants exhibit grossly wild-type organization. When compared to wild-type animals, *gcna-1(ne4356)* mutants

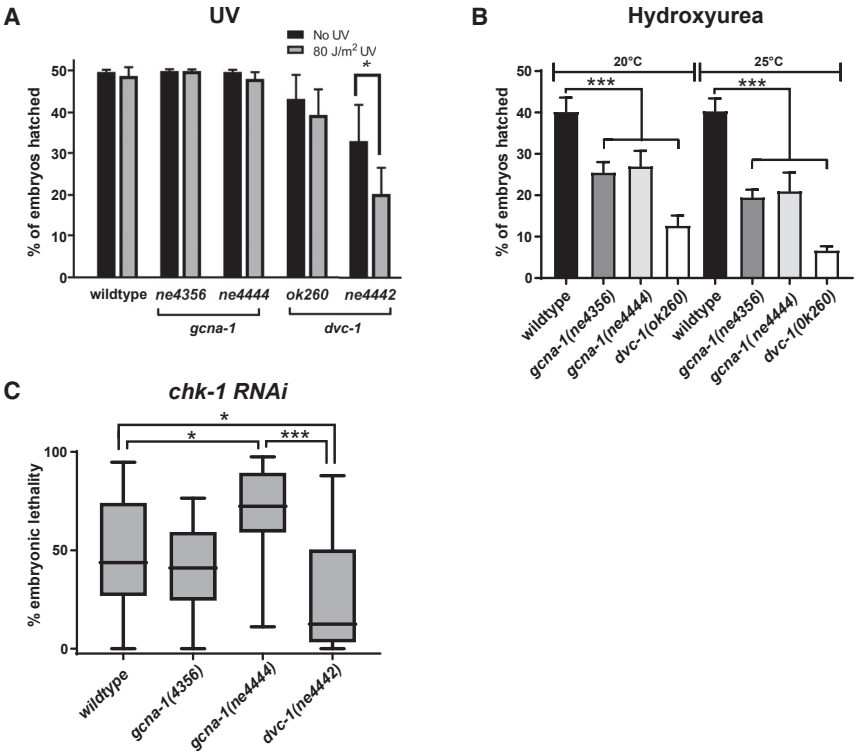

Figure 2. *gcna-1* Is Required for Response to Replication Stress

(A and B) Hatching rate of embryos after exposure of adults to UV (A) and hydroxyurea (B). Error bars, SDM.

(C) Knockdown of *chk-1* in *gcna-1* mutants results in embryonic lethality. Values are normalized to the mean hatching rate of untreated controls. Box depicts 25th and 75th percentiles, and median. Whiskers represent the minimum and maximum values. ***$p < 0.0001$, *$p < 0.05$. See also Figure S2.

displayed moderately elevated levels of germ cell apoptosis (Figure S1C).

Gradual loss of genomic or epigenetic integrity in germ cells results in sterility over successive generations, a phenotype termed "germline mortality" (Ahmed and Hodgkin, 2000; Harris et al., 2006; Meier et al., 2006). Interestingly, despite an apparently mild phenotype in early generations, *gcna-1(ne4356)* mutants have a mortal germline, where brood sizes become progressively smaller and the population fails to survive beyond 12 generations (Figure 1B), consistent with a role for GCNA-1 in maintaining germline immortality.

The GCNA-1 homolog DVC-1 is also expressed in the germline (Reinke et al., 2004). We therefore aimed to investigate whether the two genes have redundant functions. For this analysis, we used *dvc-1(ok260)*, a presumptive null allele. Consistent with parallel or redundant functions, the fertility defects in *gcna-1;dvc-1* double mutants were significantly more pronounced than in either *gcna-1* or *dvc-1* mutants alone (Figure 1A). Taken together, our results indicate that *gcna-1* and *dvc-1* have partially overlapping functions required for fertility.

gcna-1 Is Required for Response to Replication Stress

Mouse, human, and *C. elegans* SPRTN (DVC-1) orthologs are recruited to UV-induced DNA damage and are necessary for lesion bypass at stalled replication forks (Juhasz et al., 2012, Centore et al., 2012; Machida et al., 2012; Maskey et al., 2014; Mosbech et al., 2012). Hydroxyurea depletes dNTPs, stalls replication forks, increases the levels of TOP2 DPCs, and ultimately increases levels of double-strand breaks (Lee et al., 2012; Singh and Xu, 2016). Upon HU treatment, human SPRTN (DVC-1) is recruited to blocked replication forks, and *C. elegans dvc-1* mutants have higher rates of sterility compared to wild-type animals (Davis et al., 2012; Mosbech et al., 2012).

Because *gcna-1* is partially redundant with *dvc-1* for fertility, we quantified embryo hatching to compare the response of *gcna-1* and *dvc-1* mutants to exogenous DNA damage. Hatching rate is slightly, but not significantly, lower in *gcna-1* and *dvc-1* relative to wild type in the absence of drug treatment (Figure S2A). Consistent with previous reports, we observed increased sensitivity of *dvc-1* mutants to both UV and HU (Figures 2A and 2B). By contrast, *gcna-1* mutant embryos were unaffected by UV (Figure 2A), while HU increased embryonic lethality compared to wild-type controls (Figure 2B).

Checkpoint kinase, CHK-1, is critical for response to HU in *C. elegans* embryos (Brauchle et al., 2003). Even in the absence of exogenous insult, *chk-1* is required for successful DNA replication, as knockdown of *chk-1* results in embryonic lethality due to premature entry into M phase (Kalogeropoulos et al., 2004). Interestingly, SPRTN (DVC-1) is required for CHK1 activation under normal DNA replication conditions (Halder et al., 2019). We therefore asked how *dvc-1* and *gcna-1* mutants respond to RNAi-induced *chk-1* depletion. In agreement with previous reports, knockdown of *chk-1* leads to highly penetrant embryonic lethality in wild-type animals (Figure 2C). In *dvc-1* mutants, we found substantial rescue of lethality, consistent with its proposed role in activating CHK-1. However, in *gcna-1* mutants we instead observed a slight increase in lethality in a complete *gcna-1* deletion allele (*ne4444*). This differential interaction with *chk-1* suggests that unlike *dvc-1*, which functions upstream of *chk-1*, *gcna-1* likely acts downstream of the S-phase checkpoint.

Absence of *gcna-1* Causes a Potent Mutator Phenotype

We observed spontaneous mutant phenotypes during long-term culture of *gcna-1* mutant animals (Figure S1D). This observation, along with the mortal germline and *him* phenotypes (Carmell et al., 2016), could be explained by an elevated spontaneous

A

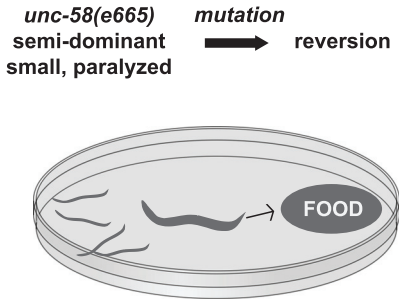

B

unc-58(e665) background	Plates with revertants/ total plates	Mutation frequency (revertants/gamete)
wildtype	1/31	3.5×10^{-6} (~1/350,000)
gcna-1(ne4356)	9/32	3.0×10^{-5} (~1/33,000)
gcna-1(ne4444)	8/24 †	3.5×10^{-5} (~1/29,000)
dvc-1(ok260)	23/29 †	1.0×10^{-4} (~1/10,000)

C

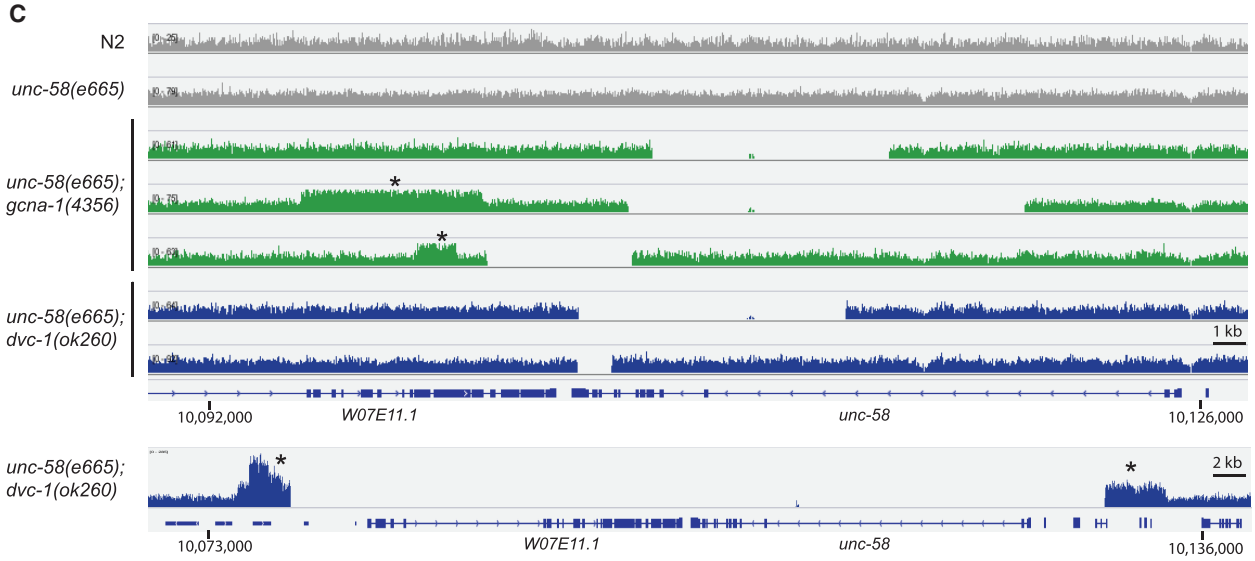

D

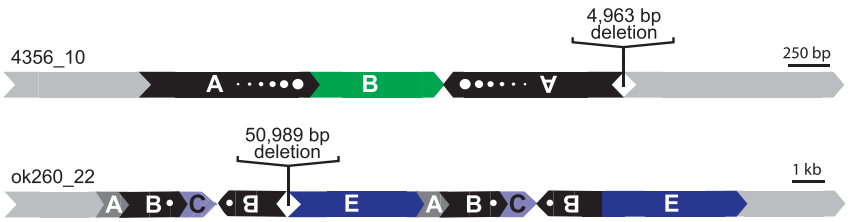

Figure 3. Absence of *gcna-1* Causes a Potent Mutator Phenotype

(A) Schematic of *unc-58(e665)* mutator assay.

(B) Frequencies of spontaneous mutation. Crosses denote >1 independent reversion event per plate, revealed by two distinct reverted phenotypes (n = 1 plate for *gcna-1(ne4444)* and n = 4 for *dvc-1(ok260)*).

(C) Sequencing coverage surrounding *unc-58* in *gcna-1* (green) and *dvc-1* (blue) mutant backgrounds. Deletions are indicated by absence of sequencing reads. Asterisks indicate increased copy number. Panel is modified from IGV.

(D) Structural rearrangements at the *unc-58* locus in revertant lines. See also Tables S2, S3, and S4 and Figures S1 and S3.

mutation frequency in the *gcna-1* germline. To explore this possibility, we carried out a genetic assay for measuring spontaneous mutations using the semi-dominant gain-of-function *unc-58(e665)* allele, which produces small, paralyzed worms (Figure 3A) (Brenner, 1974; Harris et al., 2006). The *unc-58(e665)* mutant phenotype can be suppressed by either intragenic loss of function or by extragenic mutations that are identified as animals with wild-type motility (Hodgkin, 1974). Genetic backgrounds predisposed to mutations produce more revertants than *unc-58(e665)* alone. Consistent with the idea that GCNA-1 promotes genome integrity, spontaneous revertants of *unc-58(e665)* occurred 10.6 and 12 times higher in the *gcna-1(ne4356)* and *gcna-1(ne4444)* mutant backgrounds compared to *unc-58(e665)* alone. *dvc-1(ok260)* mutants also exhibited an increased reversion rate, to 35 times higher than background (Figure 3B).

In order to determine the nature of the mutations in *unc-58* and beyond, we sequenced whole genomes of *gcna-1* and *dvc-1*

mutant revertants and examined the prevalence of structural variants, including deletions, copy number increases, inversions, and translocations. We found deletions in *unc-58* of approximately 5–13.5 kb in *gcna-1* mutants, and from 1–51 kb in *dvc-1* mutants (Figure 3C; Table S2). These deletions are consistent with those found in worms carrying mutations in DNA damage response genes using the same assay (Harris et al., 2006). Several regions adjacent to the deletions in *unc-58* had more than the expected number of sequencing reads, suggesting that *de novo* duplications had occurred. Further analysis revealed the complex nature of these duplications (Figures 3D and S3). The most complex rearrangement in *unc-58* occurred in the *dvc-1* mutant background (ok260_22), which has an inverted duplication adjacent to the breakpoint. The resultant conglomeration was then duplicated in tandem, resulting in three novel junctions in the genome (Figures 3D and S3). Similar homozygous deletions, duplications, and inversions, as well as complex rearrangements with signatures of all three, were found across the genomes of *gcna-1 and dvc-1* mutants (Tables S2 and S3). We did not find homozygous translocations between chromosomes in any of our mutant strains.

We also found hundreds of thousands of rare discordant reads in both *gcna-1* and *dvc-1* mutant lines when compared to wild-type and *unc-58(e665)* backgrounds (Table S4). In controls, 0.15% of the uniquely mapping read pairs were discordant, while mutant samples had 2-8X that amount (0.51% ± 0.1% and 0.81% ± 0.4% in *gcna-1* and *dvc-1* mutants, respectively) (Chi-squared; $p = 0$ for all pairwise comparisons). The makeup of the discordant read populations was similar across all categories between *gcna-1* and *dvc-1* mutant lines (Table S4), providing evidence for similar mutational profiles.

Interestingly, discordant reads often mapped to complex regions of the genome containing multi-copy genes, many comprising palindromes, which are inherently unstable (Tables S3 and S4). Enrichment in these regions is not likely due to a specific function for GCNA-1 and DVC-1 at these sites. Rather, it can be explained by the generally poor outcomes of DNA repair pathways in regions containing multiple homologous blocks in various orientations. The hundreds of thousands of discordant sequencing reads likely represent genuine, but rare, events in a single cell of a single worm. Such cells would likely be eliminated in the germline due to disruption of meiotic pairing and, if they survived, their genomes would likely not be compatible with embryonic development.

GCNA-1 Is Cell-Cycle Regulated and Localizes to Condensed Chromosomes during M Phase

Spartan is expressed primarily during S and G2 phases of the cell cycle; it is regulated by APC-Cdh1 and degraded in mitosis (Mosbech et al., 2012). To examine whether GCNA is also cell-cycle regulated, we analyzed GCNA levels in mouse embryonic stem (ES) cells. GCNA is lowest in G1, increases through S, and remains high in G2/M phases of the cell cycle (Figures 4A and S4A). This is consistent with GCNA localization on condensed chromosomes in mouse spermatocytes in G2 and M during meiotic prophase (Figure S5A) (Carmell et al., 2016). In *S. pombe*, studies in synchronized cells have provided finer cell-cycle resolution for GCNA and the other SprT protein, Wss1. While *wss1* transcripts rise during S and reach their highest level in G2, the GCNA ortholog, *SPBC19G7.04*, peaks in expression during M phase (Figure 4B) (Bähler, 2005).

Given the similarity between mouse and yeast cell-cycle regulation of GCNA, we examined the localization of DVC-1 and GCNA-1 in *C. elegans* using fluorescently tagged proteins and found that the two proteins had complementary localization dynamics. Specifically, when mCherry::DVC-1 was enriched in the nucleus, GFP::GCNA-1 was excluded. Upon nuclear envelope breakdown, as mCherry::DVC-1 faded, GFP::GCNA-1 became enriched on condensed chromosomes and decorated them through completion of mitosis. After mitosis, GFP::GCNA-1 was once again excluded from the DNA and replaced by nuclear mCherry::DVC-1 (Figure 4C; Video S1). An accompanying manuscript (Bhargava et al., 2019) in this issue of *Developmental Cell* confirms GCNA localization on condensed chromosomes during metaphase in *C. elegans* and also extends this observation to *Drosophila*. Taken together, comparison of GCNA cell-cycle regulation across several species revealed similar patterns, suggesting that M phase expression and chromosomal localization may be a conserved feature that distinguishes GCNA from other SprT family members and may underlie a role in DPC repair during this phase of the cell cycle.

TOP2 Co-localizes and Interacts with GCNA

Spartan and Wss1 are required for processing TOP1 DPCs (Maskey et al., 2017; Stingele et al., 2014; Vaz et al., 2016). To determine whether GCNA has similar interactions, we carried out immunoprecipitation (IP) of GCNA from UV-irradiated mouse ESCs in order to maximize the number of DPCs per cell. Following UV irradiation, GCNA relocalizes rapidly to PML (promyelocytic leukemia) bodies, which are implicated in DNA damage response (Figure S4B) (Chang et al., 2018). However, *Gcna*-mutant ESCs are not sensitized to UV, suggesting that GCNA is not absolutely required to process UV-induced lesions (Figure S4C). Nevertheless, through mass spectrometry, we identified TOP2 as an interactor of GCNA (Figure 5A; Table S5). Vertebrates encode two TOP2 isozymes termed alpha and beta. TOP2 alpha functions in chromosome condensation and segregation like the single TOP-2 in *C. elegans* and yeasts (Austin and Marsh, 1998). The majority of our peptides were derived from TOP2 alpha, but we also recovered peptides from TOP2 beta and TOP1 (Figure 5A; Table S5). Overall, GCNA ranked in the top 5% of proteins recovered when ranked by the number of exclusive spectra per protein, while TOP2 and TOP1 were in the top 15th and 40th%, respectively.

Interestingly, in yeast, worm, and mammals, TOP2 expression peaks in G2/M and localizes along condensed mitotic and meiotic chromosome axes (Gómez et al., 2014; Jaramillo-Lambert et al., 2016; Kleckner et al., 2013; Maeshima and Laemmli, 2003; Moens and Earnshaw, 1989). Thus, TOP2 and GCNA exhibit similar cell-cycle dependencies. We, therefore, carried out live-cell imaging with GFP::GCNA-1 and TOP-2::mCherry in *C. elegans* and confirmed colocalization of GCNA-1 and TOP-2 on condensed chromosomes during embryonic cell divisions (Figure 5B). In order to confirm the physical interaction between GCNA-1 and TOP-2 suggested by mass spectrometry and colocalization, we conducted co-IP experiments and detected TOP-2::mCherry in complexes isolated from GFP::GCNA-1 IP (Figure 5C). We were not able to detect

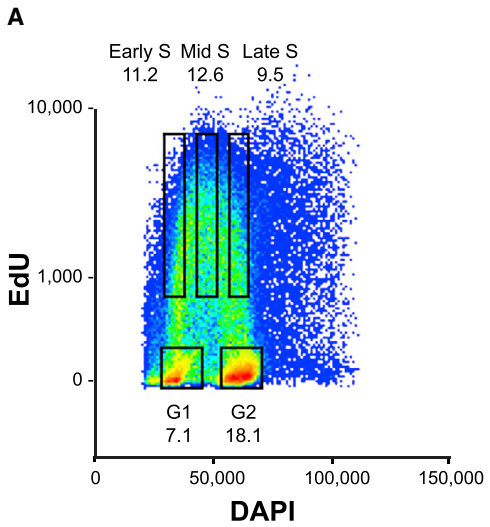

Stage	Fold increase over G1	SD
G1	1.00	0.00
Early S	1.17	0.14
Mid S	1.47	0.08
Late S	1.76	0.10
G2/M	1.75	0.12

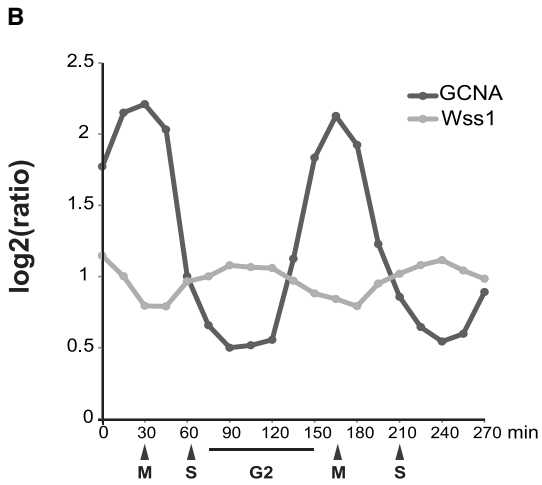

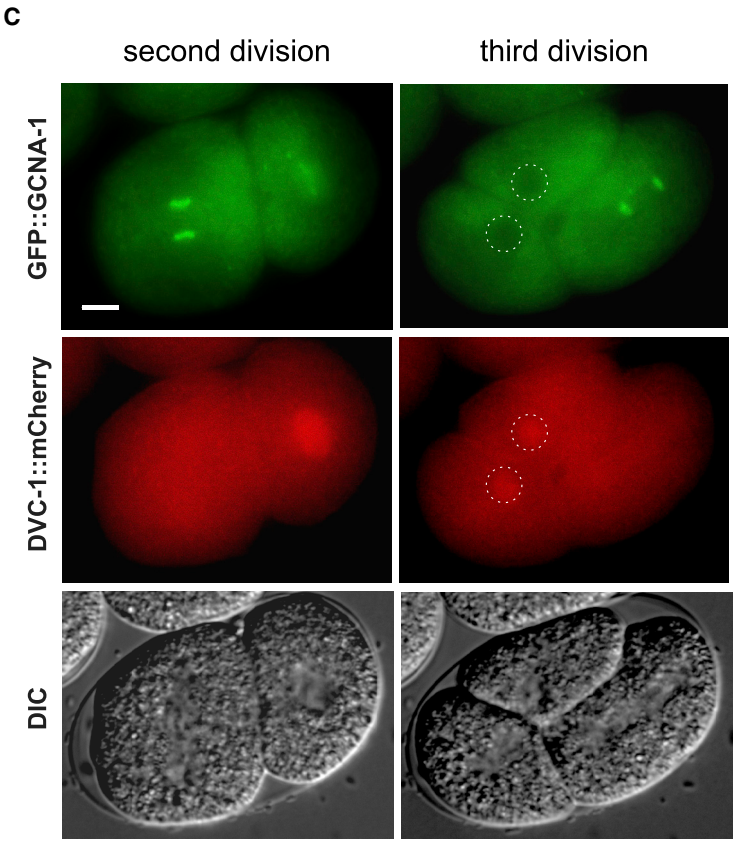

Figure 4. GCNA is Cell-Cycle Regulated and Localizes to Condensed Chromosomes during M Phase

(A) Representative flow cytometry analysis of cell cycle and GCNA expression in mouse ESCs.

(B) Cell-cycle regulated expression of *S. pombe* GCNA and *wss1* transcripts (Gene Expression Viewer, Rustici et al., 2004). The timing of mitosis (M), S, and G2 phases are indicated.

(C) Localization of GFP::GCNA-1 and DVC-1::mCherry in live *C. elegans* embryos during the second and third cell divisions. Nuclei in ABa and ABp cells are indicated by dashed circles. Scale bar, 5 μm. See also Figure S4; Video S1.

the reciprocal interaction, likely due to the large difference in abundance of the two proteins.

Of note, our TOP-2::mCherry fusion appears to be hypomorphic, as we observed chromatin bridges during mitosis in the TOP-2::mCherry line but never in a line with wild-type TOP-2 (Figures S2B and S2C). TOP2 is required for proper separation of sister chromatids in mitosis; temperature sensitive alleles of TOP2 or chemical inhibition results in the formation of anaphase chromatin bridges (Cimini et al., 1997; Uemura et al., 1987). Interestingly, GFP::GCNA-1 and TOP-2::mCherry remain on the entangled

A

Proteins Recovered in GCNA Immuno-Precipitation	% Coverage of Protein	Exclusive Spectrum Count	Exclusive Unique Peptides
GCNA	13	86	8
TOP2 alpha	17	46	18
TOP2 beta	4	1	1
TOP1	7	6	4

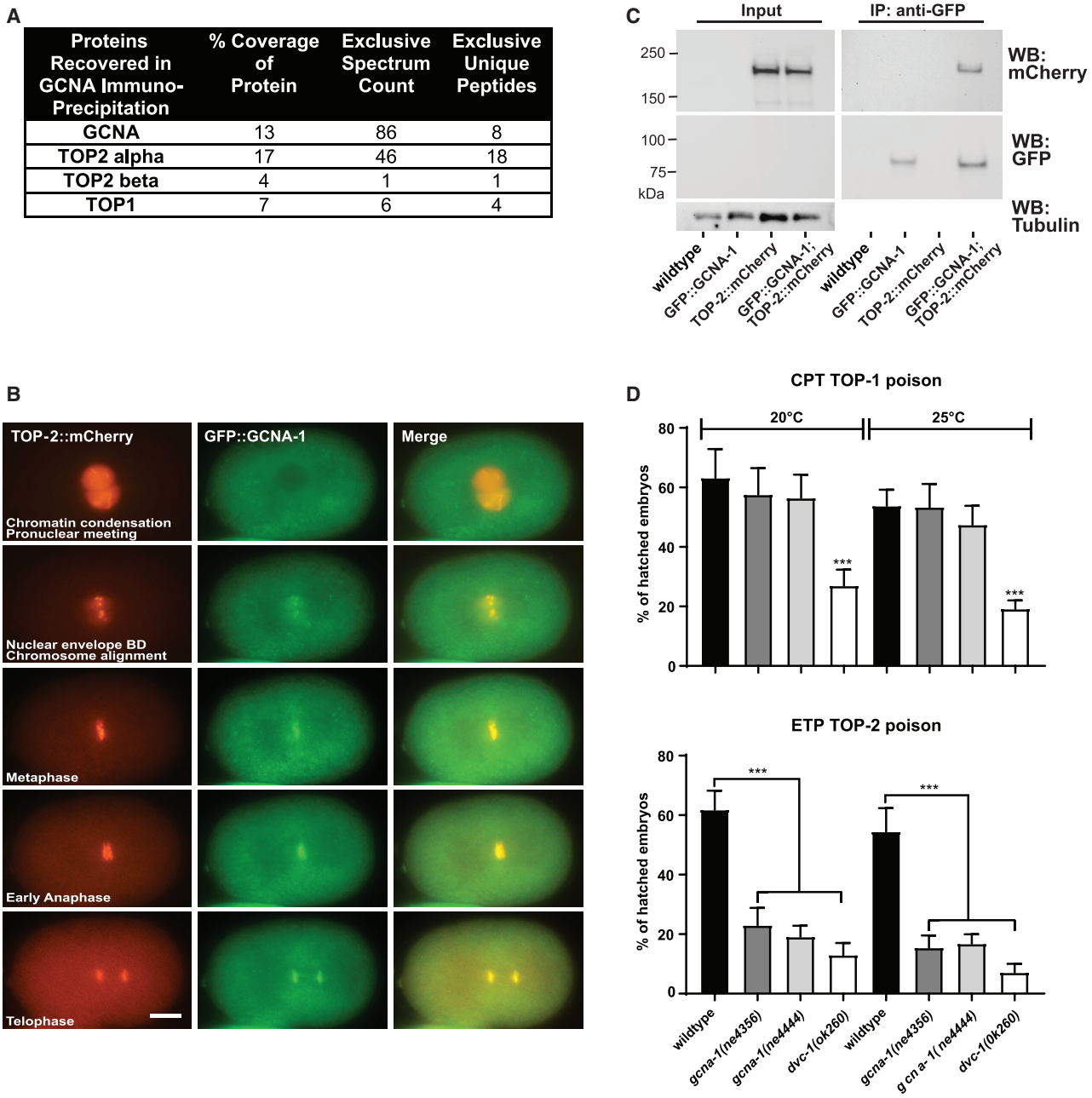

Figure 5. GCNA and TOP2 Physically Interact, Colocalize on Condensed Chromosomes, and Have a Functional Relationship

(A) Topoisomerase peptides recovered from anti-GCNA IP from mouse ESCs. Seven additional peptides are shared between TOP2 alpha and beta. No GCNA or topoisomerase peptides were recovered in an isotype control IP (Table S5).

(B) Live-cell imaging of the first embryonic cell division in *C. elegans* showing colocalization of TOP-2:mCherry and GFP::GCNA-1. Scale bar, 5 μm.

(C) Co-IP of TOP-2::mCherry with GFP::GCNA-1. Note: GFP::GCNA-1 is not abundant enough to be detected in input.

(D) Hatching rate following treatment with TOP1 (camptothecin, CPT) and TOP2 (etoposide, ETP) poisons. n = 60, error bars, SDM. ***p < 0.0001. See also Figure S2; Video S2.

DNA of bridges in this TOP-2::mCherry hypomorph (Figure S2B; Video S2), further suggesting that GCNA and TOP2 have a functional relationship. Moreover, this hypomorphic allele does not alter the localization of GCNA-1 observed during mitosis, as GFP::GCNA-1 localization in a wild-type *top-2* background (Figure 4C) is consistent with GCNA-1 localization in the hypomorph.

GCNA-1 Mutants Are Sensitive to TOP-2 but Not TOP-1 Inhibition

We sought to confirm whether the colocalization and physical interaction of GCNA and TOP2 reflects the fact that TOP2 DPCs are targets of GCNA during DPC repair. We treated worms with topoisomerase poisons and used embryo-hatching rate as

a readout of unrepaired DNA damage. *dvc-1(ok260)* worms were more sensitive to camptothecin, a TOP1 poison, than wild-type worms, while *gcna-1(ne4356)* and *gcna-1(ne4444)* worms were unaffected (Figure 5D). In contrast, treatment with the TOP2 poison etoposide revealed that mutants in both genes were sensitive to the drug (Figure 5D). Consistent with our protein interaction data from mouse ESCs, this suggests that DPCs consisting of TOP-2, and not TOP-1, are the primary target of GCNA-1 in *C. elegans*.

Gcna-Mutant Mouse Germline Defects Are Consistent with Buildup of TOP2 DPCs

In light of the connection we have drawn between GCNA-1 and TOP-2 in *C. elegans*, we examined *Gcna*-mutant mice (Carmell et al., 2016) for phenotypes consistent with defects in DPC removal. *Gcna* is expressed throughout germ cell development, including during all key events of meiosis and spermiogenesis (Enders and May, 1994). Mouse GCNA lacks the protease domain, zinc finger, and HMG box common in other family members. Nonetheless, *Gcna*-mutant male mice are sterile, indicating that GCNA has significant function that is distinct from proteolysis. Examination of the phenotypes of *Gcna*-mutant mice provided us with the opportunity to probe GCNA's non-proteolytic roles in DPC repair in isolation.

TOP2 relieves helical torsion caused by transcription machinery and is required for efficient transcription (Mondal and Parvin, 2001). We examined mRNA populations in *Gcna*-mutant testes at postnatal day 8 (p8) when mitotic spermatogonia and meiotic cells in leptotene are present, and day 18 (p18) to survey all stages of meiotic cells (Kluin et al., 1982). The first wave of spermatogenesis is developmentally distinct from adult spermatogenesis; however, examining these stages avoids the confounding effect of spermatid loss on the transcriptome in *Gcna* mutants. GCNA is similarly expressed and localized around condensed chromosomes during first wave and steady-state spermatogenesis (Figure S5A). There were essentially no changes in gene expression in *Gcna* mutants; only 33 genes differed at p8, and 80 at p18. Transposon expression also did not change (Table S6).

As TOP2 facilitates chromatin condensation and is thus is abundant during leptotene (Leduc et al., 2008), we examined *Gcna*-mutant spermatocytes for chromatin abnormalities. We found that all *Gcna*-mutant leptotene spermatocytes exhibit dramatic premature chromatin condensation when compared to controls. The chromatin in mutant cells is largely detached from the nuclear membrane, occupies only a small fraction of the nucleus, and is more compact than wild-type chromatin is at the subsequent stage of zygotene (Figures 6A and S5B). Remarkably, despite these dramatic defects, by pachytene, *Gcna*-mutant nuclei recover a nearly wild-type histological appearance (Figure S5B).

In light of the genomic instability in *C. elegans gcna-1* mutants, we examined meiotic spermatocytes of *Gcna*-mutant mice for hallmarks of DNA damage consistent with aberrant DPC repair. In wild-type leptotene and zygotene spermatocytes, the DNA damage markers gamma-H2AX, BRCA1, and ATR are found throughout the nucleus due to meiotic double-strand breaks. By pachytene, synapsis is complete, double-strand breaks have been resolved, and these proteins become enriched in the XY body, a specialized chromatin domain containing sex chromosomes (Burgoyne et al., 2007). In order to monitor meiotic prophase in *Gcna*-mutant spermatocytes, we immunostained spermatocyte spreads with an antibody recognizing SYCP3, a component of the synaptonemal complex. We also immunostained for gamma-H2AX, BRCA1, and ATR in order to detect DNA damage and asynapsed chromosomes. Surprisingly, despite dramatic chromatin condensation in all leptotene cells, 82% of pachytene (n = 142) and 89% of diplotene (n = 46) *Gcna*-mutant nuclei exhibited normal synapsis and DNA damage resolution compared to 97% and 100% of wild-type nuclei (n = 112 and 45) at the same stages (Pearson chi squared, p = 0.0005 and 0.02, respectively). Overall, 9.2% of mutant pachytene spermatocytes exhibit mild asynapsis of one or a few chromosomes accompanied DNA damage, as detected by gamma-H2AX staining, compared to 0.9% of wild-type nuclei (Figure 6B) (Pearson chi squared, p = 0.004). Nuclei with gamma-H2AX anomalies also display aberrant BRCA1 and ATR localization (Figure S5C), reflecting the fact that damage repair and synapsis are interdependent processes in mice (Inagaki et al., 2010). Interestingly, 7.7% of pachytene and 6.5% of diplotene spermatocytes in *Gcna*-mutant mice retain gamma-H2AX and ATR proteins throughout the nucleus even where synapsis has proceeded normally, indicating widespread DNA damage persists in mutants. This condition was not observed in wild-type nuclei (Pearson chi squared p = 0.00003), pointing to a role for GCNA in processing DNA damage (Figures 6B and S5C).

Topoisomerase function is required to properly execute meiotic crossovers. DPCs created by both TOP1 and TOP2 poisons are mutagenic to germ cells, causing aneuploidy due to effects on recombination (Attia et al., 2013; Marchetti et al., 2001; Russell et al., 2000, 2004). In addition, loss of function of *top2* results in decreased crossover interference in yeast (Kleckner et al., 2013). Crossover interference is the phenomenon by which the presence of a crossover decreases the probability of another occurring nearby (Hillers, 2004). One model posits that crossover interference is mediated by long distance redistribution of mechanical stress by Top2 (Zhang et al., 2014).

To determine whether mouse *Gcna* mutants have recombination defects, we immunostained spermatocyte spreads for MLH1, which marks the location of the majority of crossovers (Hassold et al., 2000). *Gcna*-mutant mice had significantly fewer MLH1 foci per nucleus, from an average of 26 in wild-type to 21 in mutant nuclei (Wilcoxon rank sum: $p < 5e{-}15$) (Figure 6Cii). Accordingly, the percentage of bivalents with no MLH1 focus increased in the mutant relative to wild type, and the percentage with two foci decreased (Figure 6Ciii).

To assess crossover interference, we measured inter-MLH1 focus distance and found significant differences in crossover distributions in the shortest chromosomes (Chr.14-19), where crossovers in the *Gcna* mutant were closer together than wild type across the entire spectrum of interfocus distances (Figure 6Civ). To quantify the degree of interference, we calculated the gamma shape parameter, where a value of 1 indicates no interference and higher values indicate stronger interference (McPeek and Speed, 1995). Mutant bivalents exhibit significantly less interference (8.498 in mutant versus 11.274 in wild type) (Two-sided Mann–Whitney; p = 0.0051). We found similar results for Chr.11-13 (Figure S6) but not for longer chromosomes. Taken

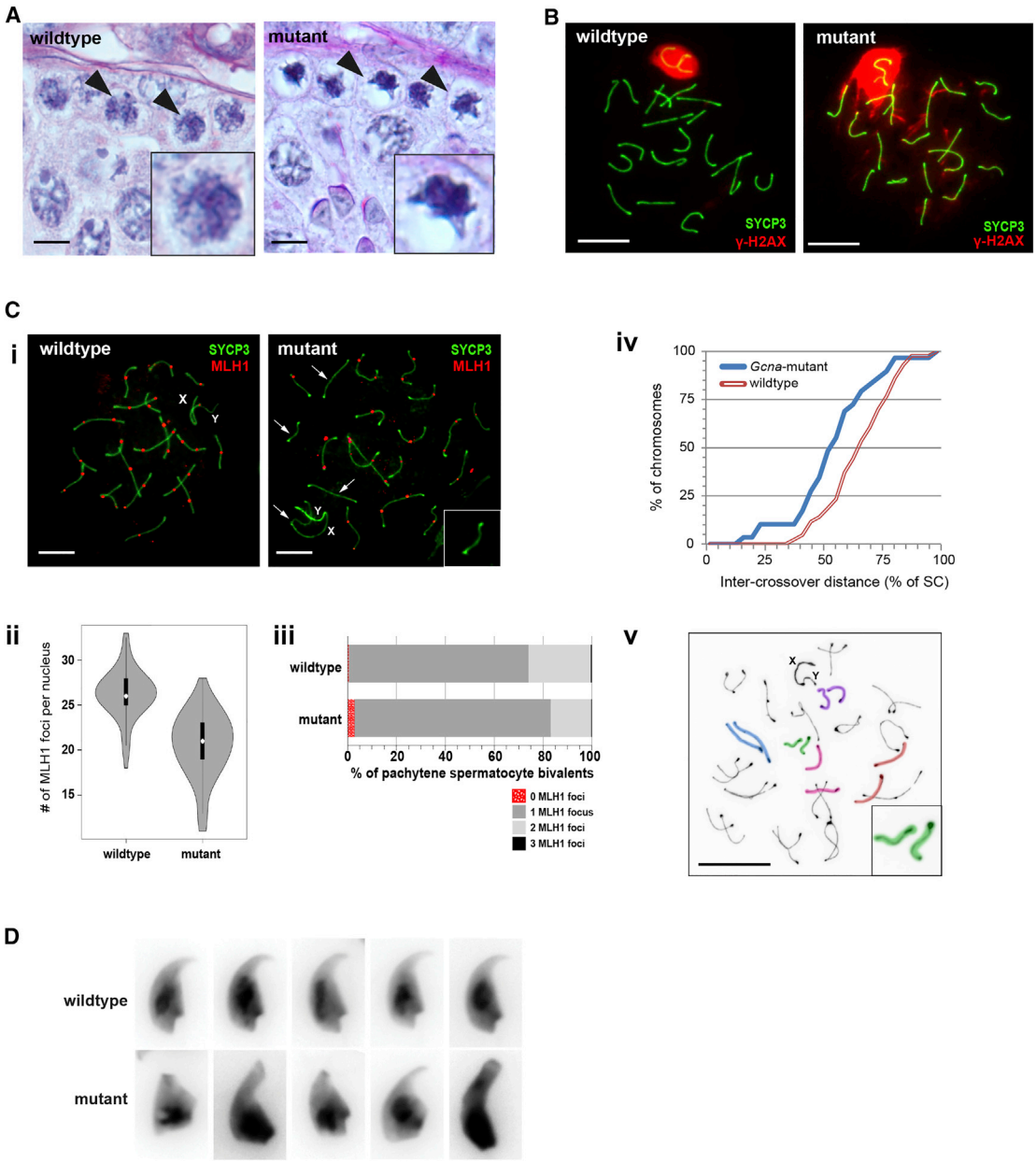

Figure 6. *Gcna*-Mutant Spermatocytes Exhibit DNA Damage, Crossover Defects, and Chromatin Condensation Abnormalities

(A) Histology of Stage IX seminiferous tubules. Representative leptotene spermatocytes are indicated by arrowheads and detailed in insets.

(B) Pachytene spermatocytes immunostained with SYCP3 (green) and γ-H2AX (red).

(C) Analysis of crossovers in *Gcna*-mutant spermatocytes. For Ci, Cii, and Ciii, n = 300 nuclei per genotype. (1) Pachytene spermatocytes stained with SYCP3 (green) and MLH1 (red). Bivalents lacking MLH1 foci are indicated by white arrows and detailed in inset. X and Y chromosomes are labeled. (2) Quantification of MLH1 foci per nucleus. (3) Pachytene bivalents with 0, 1, 2, or 3 MLH1 foci. (4) Cumulative distribution curves of the distance between MLH1 foci normalized to the length of the synaptonemal complex (SC). n > 450 chromosomes. (5) *Gcna*-mutant diplotene spermatocyte stained with SYCP3 (black). Univalent chromosome pairs are indicated by colored highlights.

(D) Morphology of DAPI-stained sperm heads. Scale bars, 5 μm. See also Figures S5 and S6.

together, our results are consistent with phenotypes caused by TOP2 DPCs. The absence of GCNA, through its effect on TOP2, may affect long distance chromatin topology that is postulated to form the basis for crossover interference.

Homologous chromosomes are held together during diplotene by chiasmata, physical connections formed by crossovers that are essential for migration toward opposite spindle poles during metaphase. Without crossovers, homolog pairs prematurely separate into univalents before metaphase, leading to missegregation. Etoposide causes TOP2 DPCs that lead to both structural and numerical chromosome aberrations in spermatocytes after the first meiotic division (Attia et al., 2002; Marchetti et al.,

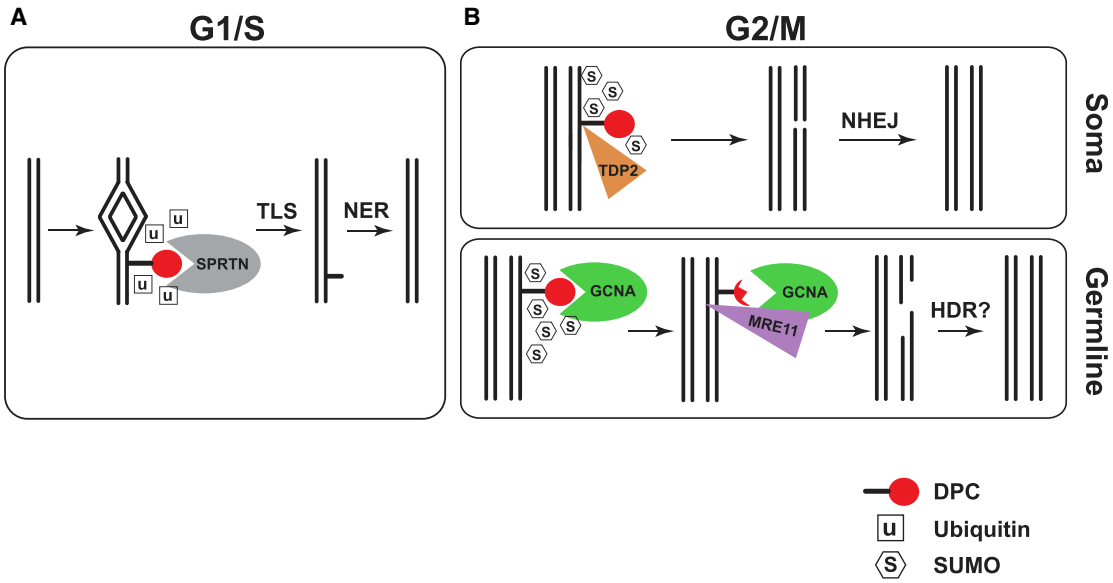

Figure 7. Proposed Model for Germline-Specific DPC Processing by GCNA

(A) In S phase in both somatic and germline cells, ubiquitin signaling leads to Spartan-mediated proteolysis of DPCs. Remnants are bypassed by TLS machinery and repaired by NER. Spartan is not present in mitosis.

(B) Outside of S, in germline and soma, DPC repair is mediated through SUMO signaling. In the soma (top), TDP2 hydrolyzes the bond between DPC and DNA and yields DNA ends predisposed to error prone NHEJ. NHEJ allows somatic cells to avoid LOH associated with HDR. In the germline (bottom), NHEJ is suppressed, and Spartan is complemented by GCNA, which recruits an MRE11-containing endonuclease complex to generate DNA ends that are compatible with HDR. Thus, germ cells can repair DPCs without risking NHEJ-associated mutations that would be detrimental to the heritable genome and incompatible with germline immortality.

2001, 2006). In order to determine whether the phenotype of *Gcna*-mutant mice is consistent with buildup of TOP2 DPCs, we examined the integrity of chromosomes in *Gcna* mutants during diplotene.

We examined at least 1,000 homolog pairs and found that *Gcna*-mutant spermatocytes presented with prematurely separated bivalents, indicating that they must lack chiasmata (Figure 6Cv). Overall, 79% of mutant nuclei had at least one univalent chromosome pair compared to 32.5% of wild-type nuclei (Fisher's exact test; $p = 4e{-}6$). Aberrant mutant spermatocytes had an average of 4 sets of univalents per nucleus, compared to 1.8 in wild type (t test; $p < 0.0005$). Of the mutant nuclei with at least one set of univalents, none affected only sex chromosomes, 36% affected only autosomes, and 64% affected both autosomes and sex chromosomes; wild-type nuclei had 21%, 43%, and 36% in each category, respectively. Fewer crossovers would cause *Gcna*-mutant spermatocytes to progress to metaphase with prematurely separated chromosomes. Nondisjunction would consequently lead to aneuploidy in gametes and likely contributes to the sterility of *Gcna*-mutant males.

TOP2 is abundantly expressed when DNA is undergoing dramatic condensation for packaging into sperm heads, up to six times more compact than in a mitotic cell (Jung et al., 2017; Leduc et al., 2008; Ward and Coffey, 1991). TOP2 and SPO11 create DNA breaks that facilitate this germ-cell specific chromatin compaction (Akematsu et al., 2017; Leduc et al., 2008; Marcon and Boissonneault, 2004; Rathke et al., 2007). Sperm in which hypercondensation has been disturbed are dramatically misshapen (Gou et al., 2017; Yuen et al., 2014). In order to determine whether *Gcna*-mutant sperm have characteristics of topoisomerase dysfunction, we examined the morphology of *Gcna*-mutant sperm and found an array of abnormal head shapes consistent with failure to execute proper sperm DNA topological rearrangements necessary for full compaction (Figure 6D).

DISCUSSION

The phylogenetic conservation and expression of GCNA proteins suggest an integral role in germ cells and multipotent cells throughout eukarya. Here, we provide evidence that GCNA promotes genome integrity in both mice and *C. elegans*. Our genetic findings suggest that GCNA-1 functions in parallel with its homolog Spartan (DVC-1) in *C. elegans*, and are consistent with a role for GCNA in the resolution of Topoisomerase 2 DNA-Protein Crosslinks. Cycling cells have a DPC burden of several thousand DPCs per cell, and a significant portion of DPCs consists of trapped topoisomerase reaction intermediates (Oleinick et al., 1987; Roca, 2009). Considering the increased requirement for topoisomerases in germ cells and embryos, it is reasonable to expect that these cells would carry an increased DPC burden, and that specialized pathways have evolved to process them.

Although Spartan has a broad range of S-phase specific functions, we find that the overlap in Spartan and GCNA phenotypes links both proteins to TOP2 DPCs. We propose a model wherein GCNA and Spartan function in parallel to promote genome integrity, with Spartan primarily active during DNA replication, and GCNA during mitosis to ensure robust resolution of DPCs prior to completion of the cell cycle (Model, Figure 7). Our model

was initially motivated by the partially overlapping phenotypes between *gcna-1* and *dvc-1* mutants, as well as the synthetic sterility phenotype of *dvc-1* and *gcna-1* in *C. elegans*. It was further supported by the complementary expression patterns of GCNA with Spartan in mice and with *wss1* in yeast, their mutually exclusive and complementary localization pattern in the *C. elegans* embryo, and genetically by the differential interaction of *gcna-1 and dvc-1* with the *chk-1* DNA damage checkpoint. Our bioinformatic analyses of *gcna-1* mutant *C. elegans* revealed a multitude of genomic alterations consistent with low fidelity repair of DNA damage in the absence of GCNA-1. Finally, our chemical biology and biochemical analyses suggest a role for GCNA in facilitating resolution of TOP2 DPCs in *C. elegans*. Although mouse GCNA is a unique family member (having lost its SprT protease domain) our genetic data nevertheless support a role for GCNA in maintaining genome integrity in the mouse germline. Specifically, the meiotic phenotypes of *Gcna*-mutant mice, including persistent DNA damage, decreased crossovers and crossover interference, and chromatin condensation defects, echo those produced by both chemical and genetic alterations that cause buildup of DPCs. Together with co-immunoprecipitation of mouse GCNA with topoisomerases, these phenotypes are suggestive of a conserved TOP2 DPC-based mechanism, though we cannot rule out the possibility that mouse GCNA promotes germline genome stability in other ways.

The key aspect of our model is that DPC resolution differs on two levels: cell-cycle phase (G1/S versus G2/M) and cell type (germline versus soma). Depending on these two criteria, DPC repair machinery is recruited by different signals (ubiquitin versus SUMO), the machinery involved differs (Spartan versus GCNA versus tyrosyl-DNA phosphodiesterase 2 [TDP2]), and downstream repair takes place through different pathways (nucleotide excision repair [NER] versus non-homologous end joining [NHEJ] versus homology-directed repair [HDR]) (Figure 7). During S phase, Spartan, which is recruited and regulated by ubiquitin, proteolytically reduces bulky DPCs to short peptides that are bypassed by the TLS machinery and later repaired by NER. This process is similar between somatic and germline cells (Figure 7A).

Outside of S phase, somatic and germ cells prefer different repair pathways. Somatic cells utilize NHEJ, which directly ligates damaged DNA ends and often results in small deletions or insertions, as it avoids the risk of introducing mitotic crossovers and associated loss of heterozygosity (LOH) (Figure 7B, top) (Lieber, 2010). In germline and stem cells, however, error-prone NHEJ is broadly suppressed in favor of far more accurate HDR (Figure 7B, bottom) (Ahmed et al., 2010; Clejan et al., 2006; Enguita-Marruedo et al., 2019; Goedecke et al., 1999; Lemmens et al., 2013; Tichy et al., 2010). Generally, TOP2 DPCs are processed through two main avenues: (1) TDP2 reverses the crosslink between TOP2 and DNA or (2) an endonuclease such as MRE11 cleaves off the modified DNA end (Aparicio et al., 2016; Cortes Ledesma et al., 2009; Hoa et al., 2016; Neale et al., 2005). The choice between these two modalities is consequential for downstream repair—TDP2-hydrolyzed DNA ends are primed for NHEJ, while MRE11 primarily feeds into HDR (Figure 7B) (Caldecott, 2012; Gomez-Herreros et al., 2013; Hoa et al., 2016; Schellenberg et al., 2012; Stingele et al., 2017; Stracker and Petrini, 2011). Consistent with the germline's predisposition toward HDR over NHEJ, TDP2 cannot hydrolyze SPO11 DPCs *in vivo* during meiotic prophase (Johnson et al., 2019). Suppression of TDP2 and/or NHEJ in germ and stem cells necessitates an alternative pathway, which we propose involves GCNA, to process DPCs and direct repair toward HDR (Figure 7B, bottom).

We find that mouse GCNA associates with the MRN components MRE11 and RAD50 (Table S5), prompting a model in which GCNA recruits MRN to cleave off GCNA-proteolyzed TOP2 DPC remnants (Figure 7B, bottom). SUMOylation regulates recruitment, activity, and stability of damage response proteins (Morris and Garvin, 2017). The MRN complex, TOP1, and TOP2 are all SUMOylated (Liao et al., 2018; Mao et al., 2000; Sohn and Hearing, 2012), and we propose that GCNA may recruit MRN via the SUMO interacting motifs embedded within the disordered domain of GCNA. GCNA-1 has recently been shown to bind polySUMO chains to facilitate germ cell and embryonic survival in response to DPC formation (Borgermann et al., 2019). TDP2 is also recruited to TOP2 DPCs via SUMOylation (Schellenberg et al., 2017), suggesting that SUMO, rather than ubiquitin, may be a universal signal for DPCs outside of S phase. In sum, we propose that a primary role of GCNA is to facilitate repair of TOP2, and possibly other DPCs, down a pathway mediated by MRN, thus, supporting HDR in germ cells and stem cells where GCNA is expressed across eukarya.

Significant additional investigation will be necessary to fully explore our model; however, the mortal germline phenotype and accumulation of deletions and rearrangements in *gcna-1* deficient worms (Figures 1B and 3) are consistent with failure of HDR-based repair in the germline (Malkova and Ira, 2013), and offer preliminary genetic support for this model. Interestingly, ectopic expression of *Gcna* in a human somatic cell line decreases proliferative capacity (Borgermann et al., 2019). The authors suggest that GCNA may be interfering with other DPC processing mechanisms; we further suggest that GCNA may be driving deleterious mitotic crossover events in a non-permissive somatic environment.

Mouse GCNA, which lacks a protease domain, zinc finger, and HMG box, and at first glance seems to be an evolutionary accident, has persisted in its current form for ~25 million years (Carmell et al., 2016). It interacts with TOP2 (Figure 5A) and retains significant function as evidenced by mutant phenotypes consistent with DPC processing defects (Figures 6 , S5, and S6). Importantly, mouse GCNA retains motifs for SUMO interaction (Carmell et al., 2016), and thus has the potential to mediate interactions with both trapped topoisomerases and with other repair machinery including the MRN complex. The phenotype of the mouse mutant may be an indicator that SUMO-mediated recruitment is as crucial to GCNA function as proteolysis. Interestingly, human Spartan mutants without protein-protein interaction domains but with intact protease domains have severe phenotypes, revealing critical non-proteolytic functions of Spartan as well (Lessel et al., 2014).

In addition to a role at DPCs, it also remains possible that mouse GCNA promotes genomic integrity through other means. Like mutations in *Gcna*, mutations in mouse *Mre11, Nbs1, and Zip4h* (members of the MRN and ZMM complexes) reveal defects in double-strand break repair, synaptonemal complex integrity, and crossover formation and interference (Adelman and Petrini, 2008; Cherry et al., 2007). As the ZMM and MRN

complexes facilitate HR-based meiotic recombination (Pyatnitskaya et al., 2019), a role for GCNA in recruiting these complexes either directly or indirectly to promote HR at meiotic double-strand breaks could underlie the phenotypic similarities.

Our data raise the intriguing possibility that *Gcna* deficiency could cause disease in humans. Human Spartan mutations cause Ruijs-Aalfs syndrome, which is associated with progeria and cancer due to DNA damage and chromosomal instability (Lessel et al., 2014; Lopez-Mosqueda et al., 2016; Maskey et al., 2014). Because *Gcna* is primarily expressed in the germline, humans carrying *Gcna* mutations are more likely to have germline than somatic phenotypes. *Gcna* is on the X chromosome, and men with mutant *Gcna* alleles may have compromised fertility and possibly be sterile. Additionally, offspring of these men could have a significant mutational load that originated in the germline of their father. Taken together, our results suggest that GCNA proteins are critical across a wide range of eukaryotic species for ensuring both short-term reproductive success and long-term fitness and survival of species.

STAR★METHODS

Detailed methods are provided in the online version of this paper and include the following:

- KEY RESOURCES TABLE
- LEAD CONTACT AND MATERIALS AVAILABILITY
- EXPERIMENTAL MODEL AND SUBJECT DETAILS
  - C. elegans Strains
  - Bacterial Strains
  - Mouse Strains
- METHOD DETAILS
  - *C. elegans* Immunohistochemistry and Embryo Analysis
  - Topoisomerase Inhibitor, UV, and Drug Treatments
  - *C. elegans* Acridine Orange Staining
  - *C. elegans* Mutator Assay
  - *C. elegans* Genomic DNA Sequencing
  - Bioinformatics
  - *C. elegans* Mortal Germline Assay
  - *C. elegans* Co-immunoprecipitation
  - C. elegans RNAi
  - *C. elegans* Brood Counts
  - Mouse Testis Histology
  - Mouse ES Cell Flow Cytometry
  - Calculation of Crossover Interference
  - RNA Sequencing
  - Mouse Spermatocyte Spreads
  - Embryonic Stem Cell Survival Assay
  - Immunoprecipitation from Mouse ES Cells
  - Mass Spectrometry
  - Microscopy
- QUANTIFICATION AND STATISTICAL ANALYSIS
- DATA AND CODE AVAILABILITY

SUPPLEMENTAL INFORMATION

Supplemental Information can be found online at https://doi.org/10.1016/j.devcel.2019.11.006.

ACKNOWLEDGMENTS

We thank S. Cheloufi, D. Bellott, D. Durning, L. Okumura, L. Teitz, and members of the Page and Mello labs for advice and discussion. We thank E. Spooner for mass spectrometry and K. Igarashi for technical assistance. We thank P. Boag and R. Pocock for access to microscopes and technical advice. Some strains provided by the CGC were supported by NIH (P40 OD010440) and the International *C. elegans* Gene Knockout Consortium. This work was supported by the Life Sciences Research Foundation to M.A.C.; American Cancer Society 129916-PF16-232-RMC to G.A.D.; and NIH grants (R37 GM058800 and P01 HD078253) to C.C.M. G.J.H. is supported by Cancer Research UK and by a Royal Society Wolfson Research Professorship. D.C.P. and C.C.M. are Howard Hughes Medical Institute Investigators.

AUTHOR CONTRIBUTIONS

Conceptualization, M.A.C. and G.A.D.; Investigation, M.A.C., G.A.D., G.M.D., P.K.N., T.E.G., L.W.M., H.R.T., D.G.D., A.D.S, M.D.E., A.R.O., and K.A.R.; Writing – Original Draft, M.A.C.; Writing – Review & Editing, M.A.C., G.A.D., G.M.D., and C.C.M.; Funding acquisition, M.A.C., G.A.D., G.M.D., D.C.P., G.J.H., and C.C.M.; Supervision, M.A.C., G.M.D., D.C.P., G.J.H., and C.C.M.

DECLARATION OF INTERESTS

The authors declare no competing interests.

Received: March 4, 2019
Revised: August 14, 2019
Accepted: November 13, 2019
Published: December 12, 2019

REFERENCES

Abyzov, A., Urban, A.E., Snyder, M., and Gerstein, M. (2011). CNVnator: an approach to discover, genotype, and characterize typical and atypical CNVs from family and population genome sequencing. Genome Res. *21*, 974–984.

Adelman, C.A., and Petrini, J.H. (2008). ZIP4H (TEX11) deficiency in the mouse impairs meiotic double strand break repair and the regulation of crossing over. PLoS Genet. *4*, e1000042.

Ahmed, E.A., Philippens, M.E., Kal, H.B., de Rooij, D.G., and de Boer, P. (2010). Genetic probing of homologous recombination and non-homologous end joining during meiotic prophase in irradiated mouse spermatocytes. Mutat. Res. *688*, 12–18.

Ahmed, S., and Hodgkin, J. (2000). MRT-2 checkpoint protein is required for germline immortality and telomere replication in C. elegans. Nature *403*, 159–164.

Akematsu, T., Fukuda, Y., Garg, J., Fillingham, J.S., Pearlman, R.E., and Loidl, J. (2017). Post-meiotic DNA double-strand breaks occur in Tetrahymena, and require topoisomerase II and Spo11. Elife *6*, e26176.

Aparicio, T., Baer, R., Gottesman, M., and Gautier, J. (2016). MRN, CtIP, and BRCA1 mediate repair of topoisomerase II-DNA adducts. J. Cell Biol. *212*, 399–408.

Attia, S.M., Ahmad, S.F., Abd-Ellah, M.F., Hamada, F.M., and Bakheet, S.A. (2013). Germ cell mutagenicity of topoisomerase I inhibitor topotecan detected in the male mouse-dominant lethal study. Food Chem. Toxicol *62*, 470–474.

Attia, S.M., Schmid, T.E., Badary, O.A., Hamada, F.M., and Adler, I.D. (2002). Molecular cytogenetic analysis in mouse sperm of chemically induced aneuploidy: studies with topoisomerase II inhibitors. Mutat. Res. *520*, 1–13.

Austin, C.A., and Marsh, K.L. (1998). Eukaryotic DNA topoisomerase II beta. BioEssays *20*, 215–226.

Bähler, J. (2005). Cell-cycle control of gene expression in budding and fission yeast. Annu. Rev. Genet. *39*, 69–94.

Balakirev, M.Y., Mullally, J.E., Favier, A., Assard, N., Sulpice, E., Lindsey, D.F., Rulina, A.V., Gidrol, X., and Wilkinson, K.D. (2015). Wss1 metalloprotease partners with Cdc48/Doa1 in processing genotoxic SUMO conjugates. Elife *4*, e06763.

Bao, W., Kojima, K.K., and Kohany, O. (2015). Repbase update, a database of repetitive elements in eukaryotic genomes. Mob. DNA *6*, 11.

Barker, S., Weinfeld, M., and Murray, D. (2005). DNA-protein crosslinks: their induction, repair, and biological consequences. Mutat. Res. *589*, 111–135.

Bhargava, V., Goldstein, C.D., Russell, L., Xu, L., Ahmed, M., Li, W., Casey, A., Servage, K., Kollipara, R., Picciarelli, Z., et al. (2019). GCNA Preserves Genome Integrity and Fertility across Species. Dev. Cell *52*, this issue, 38–52.

Boag, P.R., Nakamura, A., and Blackwell, T.K. (2005). A conserved RNA-protein complex component involved in physiological germline apoptosis regulation in C. elegans. Development *132*, 4975–4986.

Boeva, V., Popova, T., Bleakley, K., Chiche, P., Cappo, J., Schleiermacher, G., Janoueix-Lerosey, I., Delattre, O., and Barillot, E. (2012). Control-FREEC: a tool for assessing copy number and allelic content using next-generation sequencing data. Bioinformatics *28*, 423–425.

Borgermann, N., Ackermann, L., Schwertman, P., Hendriks, I.A., Thijssen, K., Liu, J.C., Lans, H., Nielsen, M.L., and Mailand, N. (2019). SUMOylation promotes protective responses to DNA-protein crosslinks. EMBO J *38*, e101496.

Brangwynne, C.P., Eckmann, C.R., Courson, D.S., Rybarska, A., Hoege, C., Gharakhani, J., Jülicher, F., and Hyman, A.A. (2009). Germline P granules are liquid droplets that localize by controlled dissolution/condensation. Science *324*, 1729–1732.

Brauchle, M., Baumer, K., and Gönczy, P. (2003). Differential activation of the DNA replication checkpoint contributes to asynchrony of cell division in C. elegans embryos. Curr. Biol. *13*, 819–827.

Brenner, S. (1974). The genetics of Caenorhabditis elegans. Genetics *77*, 71–94.

Burgoyne, P.S., Mahadevaiah, S.K., and Turner, J.M. (2007). The management of DNA double-strand breaks in mitotic G2, and in mammalian meiosis viewed from a mitotic G2 perspective. BioEssays *29*, 974–986.

Caldecott, K.W. (2012). Tyrosyl DNA phosphodiesterase 2, an enzyme fit for purpose. Nat. Struct. Mol. Biol. *19*, 1212–1213.

Carmell, M.A., Dokshin, G.A., Skaletsky, H., Hu, Y.C., van Wolfswinkel, J.C., Igarashi, K.J., Bellott, D.W., Nefedov, M., Reddien, P.W., Enders, G.C., et al. (2016). A widely employed germ cell marker is an ancient disordered protein with reproductive functions in diverse eukaryotes. Elife *5*, e19993.

Centore, R.C., Yazinski, S.A., Tse, A., and Zou, L. (2012). Spartan/C1orf124, a Reader of PCNA Ubiquitylation and a Regulator of UV-Induced DNA Damage Response. Molecular Cell *46*, 625–635.

Cerutti, H., and Casas-Mollano, J.A. (2006). On the origin and functions of RNA-mediated silencing: from protists to man. Curr. Genet. *50*, 81–99.

Champoux, J.J. (2001). DNA topoisomerase I-mediated nicking of circular duplex DNA. Methods Mol. Biol. *95*, 81–87.

Chang, H.R., Munkhjargal, A., Kim, M.J., Park, S.Y., Jung, E., Ryu, J.H., Yang, Y., Lim, J.S., and Kim, Y. (2018). The functional roles of PML nuclear bodies in genome maintenance. Mutat. Res. *809*, 99–107.

Chen, S., Zhou, Y., Chen, Y., and Gu, J. (2018). fastp: an ultra-fast all-in-one FASTQ preprocessor. Bioinformatics *34*, i884–i890.

Chen, X., Schulz-Trieglaff, O., Shaw, R., Barnes, B., Schlesinger, F., Källberg, M., Cox, A.J., Kruglyak, S., and Saunders, C.T. (2016). Manta: rapid detection of structural variants and indels for germline and cancer sequencing applications. Bioinformatics *32*, 1220–1222.

Cherry, S.M., Adelman, C.A., Theunissen, J.W., Hassold, T.J., Hunt, P.A., and Petrini, J.H. (2007). The Mre11 complex influences DNA repair, synapsis, and crossing over in murine meiosis. Curr. Biol. *17*, 373–378.

Cimini, D., Antoccia, A., Tanzarella, C., and Degrassi, F. (1997). Topoisomerase II inhibition in mitosis produces numerical and structural chromosomal aberrations in human fibroblasts. Cytogenet. Cell Genet. *76*, 61–67.

Clejan, I., Boerckel, J., and Ahmed, S. (2006). Developmental modulation of nonhomologous end joining in Caenorhabditis elegans. Genetics *173*, 1301–1317.

Cortes Ledesma, F., El Khamisy, S.F., Zuma, M.C., Osborn, K., and Caldecott, K.W. (2009). A human 5′-tyrosyl DNA phosphodiesterase that repairs topoisomerase-mediated DNA damage. Nature *461*, 674–678.

Davis, E.J., Lachaud, C., Appleton, P., Macartney, T.J., Näthke, I., and Rouse, J. (2012). DVC1 (C1orf124) recruits the p97 protein segregase to sites of DNA damage. Nat. Struct. Mol. Biol. *19*, 1093–1100.

Dawson, J.A., Methven-Kelley, C., and Davis, G.M. (2017). atz-1 Influences meiosis to maintain germline chromosomal stability in Caenorhabditis elegans. Cell Biol. Int *41*, 1160–1168.

de Boer, E., Stam, P., Dietrich, A.J., Pastink, A., and Heyting, C. (2006). Two levels of interference in mouse meiotic recombination. Proc. Natl. Acad. Sci. USA *103*, 9607–9612.

Deweese, J.E., and Osheroff, N. (2009). The DNA cleavage reaction of topoisomerase II: wolf in sheep's clothing. Nucleic Acids Res. *37*, 738–748.

DiNardo, S., Voelkel, K., and Sternglanz, R. (1984). DNA topoisomerase II mutant of Saccharomyces cerevisiae: topoisomerase II is required for segregation of daughter molecules at the termination of DNA replication. Proc. Natl. Acad. Sci. USA *81*, 2616–2620.

Dokshin, G.A., Ghanta, K.S., Piscopo, K.M., and Mello, C.C. (2018). Robust genome editing with short single-stranded and long, partially single-stranded DNA donors in Caenorhabditis elegans. Genetics *210*, 781–787.

Enders, G.C., and May, J.J., 2nd (1994). Developmentally regulated expression of a mouse germ cell nuclear antigen examined from embryonic day 11 to adult in male and female mice. Dev. Biol. *163*, 331–340.

Enguita-Marruedo, A., Martín-Ruiz, M., García, E., Gil-Fernández, A., Parra, M.T., Viera, A., Rufas, J.S., and Page, J. (2019). Transition from a meiotic to a somatic-like DNA damage response during the pachytene stage in mouse meiosis. PLoS Genet. *15*, e1007439.

Fielden, J., Ruggiano, A., Popović, M., and Ramadan, K. (2018). DNA protein crosslink proteolysis repair: from yeast to premature ageing and cancer in humans. DNA Repair (Amst) *71*, 198–204.

Ghosal, G., Leung, J.W., Nair, B.C., Fong, K.W., and Chen, J. (2012). Proliferating cell nuclear antigen (PCNA)-binding protein C1orf124 is a regulator of translesion synthesis. J. Biol. Chem. *287*, 34225–34233.

Goedecke, W., Eijpe, M., Offenberg, H.H., van Aalderen, M., and Heyting, C. (1999). Mre11 and Ku70 interact in somatic cells, but are differentially expressed in early meiosis. Nat. Genet. *23*, 194–198.

Gómez, R., Viera, A., Berenguer, I., Llano, E., Pendás, A.M., Barbero, J.L., Kikuchi, A., and Suja, J.A. (2014). Cohesin removal precedes topoisomerase IIα-dependent decatenation at centromeres in male mammalian meiosis II. Chromosoma *123*, 129–146.

Gómez-Herreros, F., Romero-Granados, R., Zeng, Z., Alvarez-Quilón, A., Quintero, C., Ju, L., Umans, L., Vermeire, L., Huylebroeck, D., Caldecott, K.W., and Cortés-Ledesma, F. (2013). TDP2-dependent non-homologous end-joining protects against topoisomerase II-induced DNA breaks and genome instability in cells and in vivo. PLoS Genet. *9*, e1003226.

Gou, L.T., Kang, J.Y., Dai, P., Wang, X., Li, F., Zhao, S., Zhang, M., Hua, M.M., Lu, Y., Zhu, Y., et al. (2017). Ubiquitination-deficient mutations in human Piwi cause male infertility by impairing histone-to-protamine exchange during spermiogenesis. Cell *169*, 1090–1104.e13.

Harris, J., Lowden, M., Clejan, I., Tzoneva, M., Thomas, J.H., Hodgkin, J., and Ahmed, S. (2006). Mutator phenotype of Caenorhabditis elegans DNA damage checkpoint mutants. Genetics *174*, 601–616.

Hartsuiker, E., Bähler, J., and Kohli, J. (1998). The role of topoisomerase II in meiotic chromosome condensation and segregation in Schizosaccharomyces pombe. Mol. Biol. Cell *9*, 2739–2750.

Hassold, T., Sherman, S., and Hunt, P. (2000). Counting cross-overs: characterizing meiotic recombination in mammals. Hum. Mol. Genet. *9*, 2409–2419.

Hendzel, M.J., Wei, Y., Mancini, M.A., Van Hooser, A., Ranalli, T., Brinkley, B.R., Bazett-Jones, D.P., and Allis, C.D. (1997). Mitosis-specific phosphorylation of histone H3 initiates primarily within pericentromeric heterochromatin during G2 and spreads in an ordered fashion coincident with mitotic chromosome condensation. Chromosoma *106*, 348–360.

Hillers, K.J. (2004). Crossover interference. Curr. Biol. *14*, R1036–R1037.

Hoa, N.N., Shimizu, T., Zhou, Z.W., Wang, Z.Q., Deshpande, R.A., Paull, T.T., Akter, S., Tsuda, M., Furuta, R., Tsutsui, K., et al. (2016). Mre11 is essential for

the removal of lethal topoisomerase 2 covalent cleavage complexes. Mol. Cell *64*, 1010.

Hodgkin, J. , 1974. Genetic and anatomical aspects of the Caenorhabditis elegans male (PhD Thesis, Darwin College, Cambridge UK).

Hughes, S.E., and Hawley, R.S. (2014). Topoisomerase II is required for the proper separation of heterochromatic regions during Drosophila melanogaster female meiosis. PLoS Genet. *10*, e1004650.

Inagaki, A., Schoenmakers, S., and Baarends, W.M. (2010). DNA double strand break repair, chromosome synapsis and transcriptional silencing in meiosis. Epigenetics *5*, 255–266.

Jaramillo-Lambert, A., Fabritius, A.S., Hansen, T.J., Smith, H.E., and Golden, A. (2016). The identification of a novel mutant allele of topoisomerase II in Caenorhabditis elegans reveals a unique role in chromosome segregation during spermatogenesis. Genetics *204*, 1407–1422.

Johnson, D., Allison, R.M., Cannavo, E., Cejka, P., and Neale, M.J. (2019). Removal of Spo11 from meiotic DNA breaks in vitro but not in vivo by tyrosyl DNA phosphodiesterase 2. bioRxiv. https://doi.org/10.1101/527333.

Juhasz, S., Balogh, D., Hajdu, I., Burkovics, P., Villamil, M.A., Zhuang, Z., and Haracska, L. (2012). Characterization of human Spartan/C1orf124, an ubiquitin-PCNA interacting regulator of DNA damage tolerance. Nucleic Acids Res. *40*, 10795–10808.

Juliano, C., Wang, J., and Lin, H. (2011). Uniting germline and stem cells: the function of Piwi proteins and the piRNA pathway in diverse organisms. Annu. Rev. Genet. *45*, 447–469.

Juliano, C.E., Swartz, S.Z., and Wessel, G.M. (2010). A conserved germline multipotency program. Development *137*, 4113–4126.

Jung, Y.H., Sauria, M.E.G., Lyu, X., Cheema, M.S., Ausio, J., Taylor, J., and Corces, V.G. (2017). Chromatin states in mouse sperm correlate with embryonic and adult regulatory landscapes. Cell Rep *18*, 1366–1382.

Kalogeropoulos, N., Christoforou, C., Green, A.J., Gill, S., and Ashcroft, N.R. (2004). chk-1 is an essential gene and is required for an S-M checkpoint during early embryogenesis. Cell Cycle *3*, 1196–1200.

Keeney, S., Giroux, C.N., and Kleckner, N. (1997). Meiosis-specific DNA double-strand breaks are catalyzed by Spo11, a member of a widely conserved protein family. Cell *88*, 375–384.

Kleckner, N., Zickler, D., and Witz, G. (2013). Molecular biology. Chromosome capture brings it all together. Science *342*, 940–941.

Kluin, P.M., Kramer, M.F., and de Rooij, D.G. (1982). Spermatogenesis in the immature mouse proceeds faster than in the adult. Int. J. Androl. *5*, 282–294.

Koboldt, D.C., Zhang, Q., Larson, D.E., Shen, D., McLellan, M.D., Lin, L., Miller, C.A., Mardis, E.R., Ding, L., and Wilson, R.K. (2012). VarScan 2: somatic mutation and copy number alteration discovery in cancer by exome sequencing. Genome Res. *22*, 568–576.

Langmead, B., Trapnell, C., Pop, M., and Salzberg, S.L. (2009). Ultrafast and memory-efficient alignment of short DNA sequences to the human genome. Genome Biol. *10*, R25.

Leduc, F., Maquennehan, V., Nkoma, G.B., and Boissonneault, G. (2008). DNA damage response during chromatin remodeling in elongating spermatids of mice. Biol. Reprod *78*, 324–332.

Lee, K.C., Padget, K., Curtis, H., Cowell, I.G., Moiani, D., Sondka, Z., Morris, N.J., Jackson, G.H., Cockell, S.J., Tainer, J.A., et al. (2012). MRE11 facilitates the removal of human topoisomerase II complexes from genomic DNA. Biol. Open *1*, 863–873.

Lemmens, B.B., Johnson, N.M., and Tijsterman, M. (2013). COM-1 promotes homologous recombination during Caenorhabditis elegans meiosis by antagonizing Ku-mediated non-homologous end joining. PLoS Genet. *9*, e1003276.

Lessel, D., Vaz, B., Halder, S., Lockhart, P.J., Marinovic-Terzic, I., Lopez-Mosqueda, J., Philipp, M., Sim, J.C., Smith, K.R., Oehler, J., et al. (2014). Mutations in SPRTN cause early onset hepatocellular carcinoma, genomic instability and progeroid features. Nat. Genet. *46*, 1239–1244.

Li, H. (2013). Aligning sequence reads, clone sequences and assembly contigs with BWA-MEM. arXiv:1303.3997v2 [q-bio.GN].

Li, X.M., Yu, C., Wang, Z.W., Zhang, Y.L., Liu, X.M., Zhou, D., Sun, Q.Y., and Fan, H.Y. (2013). DNA topoisomerase II is dispensable for oocyte meiotic resumption but is essential for meiotic chromosome condensation and separation in mice. Biol. Reprod. *89*, 118.

Liao, C., Beveridge, R., Hudson, J.J.R., Parker, J.D., Chiang, S.C., Ray, S., Ashour, M.E., Sudbery, I., Dickman, M.J., and El-Khamisy, S.F. (2018). UCHL3 regulates topoisomerase-induced chromosomal break repair by controlling TDP1 proteostasis. Cell Rep. *23*, 3352–3365.

Lieber, M.R. (2010). The mechanism of double-strand DNA break repair by the nonhomologous DNA end-joining pathway. Annu. Rev. Biochem *79*, 181–211.

Lopez-Mosqueda, J., Maddi, K., Prgomet, S., Kalayil, S., Marinovic-Terzic, I., Terzic, J., and Dikic, I. (2016). SPRTN is a mammalian DNA-binding metalloprotease that resolves DNA-protein crosslinks. Elife *5*, e21491.

Machida, Y., Kim, M.S., and Machida, Y.J. (2012). Spartan/C1orf124 is important to prevent UV-induced mutagenesis. Cell Cycle *11*, 3395–3402.

MacQueen, A.J., and Villeneuve, A.M. (2001). Nuclear reorganization and homologous chromosome pairing during meiotic prophase require C. elegans chk-2. Genes Dev. *15*, 1674–1687.

Maeshima, K., and Laemmli, U.K. (2003). A two-step scaffolding model for mitotic chromosome assembly. Dev. Cell *4*, 467–480.

Malkova, A., and Ira, G. (2013). Break-induced replication: functions and molecular mechanism. Curr. Opin. Genet. Dev. *23*, 271–279.

Mao, Y., Desai, S.D., and Liu, L.F. (2000). SUMO-1 conjugation to human DNA topoisomerase II isozymes. J. Biol. Chem. *275*, 26066–26073.

Marchetti, F., Bishop, J.B., Lowe, X., Generoso, W.M., Hozier, J., and Wyrobek, A.J. (2001). Etoposide induces heritable chromosomal aberrations and aneuploidy during male meiosis in the mouse. Proc. Natl. Acad. Sci. USA *98*, 3952–3957.

Marchetti, F., Pearson, F.S., Bishop, J.B., and Wyrobek, A.J. (2006). Etoposide induces chromosomal abnormalities in mouse spermatocytes and stem cell spermatogonia. Hum. Reprod. *21*, 888–895.

Marcon, L., and Boissonneault, G. (2004). Transient DNA strand breaks during mouse and human spermiogenesis new insights in stage specificity and link to chromatin remodeling. Biol. Reprod. *70*, 910–918.

Maskey, R.S., Flatten, K.S., Sieben, C.J., Peterson, K.L., Baker, D.J., Nam, H.J., Kim, M.S., Smyrk, T.C., Kojima, Y., Machida, Y., et al. (2017). Spartan deficiency causes accumulation of topoisomerase 1 cleavage complexes and tumorigenesis. Nucleic Acids Res. *45*, 4564–4576.

Maskey, R.S., Kim, M.S., Baker, D.J., Childs, B., Malureanu, L.A., Jeganathan, K.B., Machida, Y., van Deursen, J.M., and Machida, Y.J. (2014). Spartan deficiency causes genomic instability and progeroid phenotypes. Nat. Commun. *5*, 5744.

McKenna, A., Hanna, M., Banks, E., Sivachenko, A., Cibulskis, K., Kernytsky, A., Garimella, K., Altshuler, D., Gabriel, S., Daly, M., et al. (2010). The Genome analysis toolkit: a MapReduce framework for analyzing next-generation DNA sequencing data. Genome Res. *20*, 1297–1303.

McPeek, M.S., and Speed, T.P. (1995). Modeling interference in genetic recombination. Genetics *139*, 1031–1044.

Meier, B., Clejan, I., Liu, Y., Lowden, M., Gartner, A., Hodgkin, J., and Ahmed, S. (2006). trt-1 is the Caenorhabditis elegans catalytic subunit of telomerase. PLoS Genet. *2*, e18.

Mengoli, V., Bucciarelli, E., Lattao, R., Piergentili, R., Gatti, M., and Bonaccorsi, S. (2014). The analysis of mutant alleles of different strength reveals multiple functions of topoisomerase 2 in regulation of Drosophila chromosome structure. PLoS Genet. *10*, e1004739.

Moens, P.B., and Earnshaw, W.C. (1989). Anti-topoisomerase II recognizes meiotic chromosome cores. Chromosoma *98*, 317–322.

Mondal, N., and Parvin, J.D. (2001). DNA topoisomerase IIalpha is required for RNA polymerase II transcription on chromatin templates. Nature *413*, 435–438.

Mórocz, M., Zsigmond, E., Tóth, R., Enyedi, M.Z., Pintér, L., and Haracska, L. (2017). DNA-dependent protease activity of human Spartan facilitates

replication of DNA-protein crosslink-containing DNA. Nucleic Acids Res. *45*, 3172–3188.

Morris, J.R., and Garvin, A.J. (2017). SUMO in the DNA double-stranded break response: similarities, differences, and cooperation with ubiquitin. J. Mol. Biol. *429*, 3376–3387.

Mosbech, A., Gibbs-Seymour, I., Kagias, K., Thorslund, T., Beli, P., Povlsen, L., Nielsen, S.V., Smedegaard, S., Sedgwick, G., Lukas, C., et al. (2012). DVC1 (C1orf124) is a DNA damage-targeting p97 adaptor that promotes ubiquitin-dependent responses to replication blocks. Nat. Struct. Mol. Biol. *19*, 1084–1092.

Nakano, T., Miyamoto-Matsubara, M., Shoulkamy, M.I., Salem, A.M., Pack, S.P., Ishimi, Y., and Ide, H. (2013). Translocation and stability of replicative DNA helicases upon encountering DNA-protein cross-links. J. Biol. Chem. *288*, 4649–4658.

Nakano, T., Ouchi, R., Kawazoe, J., Pack, S.P., Makino, K., and Ide, H. (2012). T7 RNA polymerases backed up by covalently trapped proteins catalyze highly error prone transcription. J. Biol. Chem. *287*, 6562–6572.

Neale, M.J., Pan, J., and Keeney, S. (2005). Endonucleolytic processing of covalent protein-linked DNA double-strand breaks. Nature *436*, 1053–1057.

Oleinick, N.L., Chiu, S.M., Ramakrishnan, N., and Xue, L.Y. (1987). The formation, identification, and significance of DNA-protein cross-links in mammalian cells. Br. J. Cancer Suppl. *8*, 135–140.

Olshen, A.B., Venkatraman, E.S., Lucito, R., and Wigler, M. (2004). Circular binary segmentation for the analysis of array-based DNA copy number data. Biostatistics *5*, 557–572.

Peters, A.H., Plug, A.W., van Vugt, M.J., and de Boer, P. (1997). A drying-down technique for the spreading of mammalian meiocytes from the male and female germline. Chromosome Res. *5*, 66–68.

Pyatnitskaya, A., Borde, V., and De Muyt, A. (2019). Crossing and zipping: molecular duties of the ZMM proteins in meiosis. Chromosoma *128*, 181–198.

Rathke, C., Baarends, W.M., Jayaramaiah-Raja, S., Bartkuhn, M., Renkawitz, R., and Renkawitz-Pohl, R. (2007). Transition from a nucleosome-based to a protamine-based chromatin configuration during spermiogenesis in Drosophila. J. Cell Sci. *120*, 1689–1700.

Reinke, V., Gil, I.S., Ward, S., and Kazmer, K. (2004). Genome-wide germline-enriched and sex-biased expression profiles in Caenorhabditis elegans. Development *131*, 311–323.

Roberts, A., and Pachter, L. (2013). Streaming fragment assignment for real-time analysis of sequencing experiments. Nat. Methods *10*, 71–73.

Robinson, J.T., Thorvaldsdóttir, H., Winckler, W., Guttman, M., Lander, E.S., Getz, G., and Mesirov, J.P. (2011). Integrative genomics viewer. Nat. Biotechnol *29*, 24–26.

Robinson, M.D., McCarthy, D.J., and Smyth, G.K. (2010). edgeR: a Bioconductor package for differential expression analysis of digital gene expression data. Bioinformatics *26*, 139–140.

Roca, J. (2009). Topoisomerase II: a fitted mechanism for the chromatin landscape. Nucleic Acids Res. *37*, 721–730.

Russell, L.B., Hunsicker, P.R., Hack, A.M., and Ashley, T. (2000). Effect of the topoisomerase-II inhibitor etoposide on meiotic recombination in male mice. Mutat. Res. *464*, 201–212.

Russell, L.B., Hunsicker, P.R., Kerley, M., Pyle, A., and Saxton, A.M. (2004). Etoposide exposure during male mouse pachytene has complex effects on crossing-over and causes nondisjunction. Mutat. Res. *565*, 61–77.

Rustici, G., Mata, J., Kivinen, K., Lió, P., Penkett, C.J., Burns, G., Hayles, J., Brazma, A., Nurse, P., and Bähler, J. (2004). Periodic gene expression program of the fission yeast cell cycle. Nat. Genet. *36*, 809–817.

Schellenberg, M.J., Appel, C.D., Adhikari, S., Robertson, P.D., Ramsden, D.A., and Williams, R.S. (2012). Mechanism of repair of 5′-topoisomerase II-DNA adducts by mammalian tyrosyl-DNA phosphodiesterase 2. Nat. Struct. Mol. Biol. *19*, 1363–1371.

Schellenberg, M.J., Lieberman, J.A., Herrero-Ruiz, A., Butler, L.R., Williams, J.G., Muñoz-Cabello, A.M., Mueller, G.A., London, R.E., Cortés-Ledesma, F., and Williams, R.S. (2017). ZATT (ZNF451)-mediated resolution of topoisomerase 2 DNA-protein cross-links. Science *357*, 1412–1416.

Shabalina, S.A., and Koonin, E.V. (2008). Origins and evolution of eukaryotic RNA interference. Trends Ecol. Evol. (Amst.) *23*, 578–587.

Singh, A., and Xu, Y.J. (2016). The cell killing mechanisms of hydroxyurea. Genes (Basel) *7*, E99.

Sohn, S.Y., and Hearing, P. (2012). Adenovirus regulates SUMOylation of Mre11-Rad50-Nbs1 components through a paralog-specific mechanism. J. Virol *86*, 9656–9665.

Stingele, J., Bellelli, R., Alte, F., Hewitt, G., Sarek, G., Maslen, S.L., Tsutakawa, S.E., Borg, A., Kjær, S., Tainer, J.A., et al. (2016). Mechanism and regulation of DNA-protein crosslink repair by the DNA-dependent metalloprotease SPRTN. Mol. Cell *64*, 688–703.

Stingele, J., Bellelli, R., and Boulton, S.J. (2017). Mechanisms of DNA-protein crosslink repair. Nat. Rev. Mol. Cell Biol. *18*, 563–573.

Stingele, J., Habermann, B., and Jentsch, S. (2015). DNA-protein crosslink repair: proteases as DNA repair enzymes. Trends Biochem. Sci. *40*, 67–71.

Stingele, J., Schwarz, M.S., Bloemeke, N., Wolf, P.G., and Jentsch, S. (2014). A DNA-dependent protease involved in DNA-protein crosslink repair. Cell *158*, 327–338.

Stracker, T.H., and Petrini, J.H. (2011). The MRE11 complex: starting from the ends. Nat. Rev. Mol. Cell Biol. *12*, 90–103.

Halder, S., Torrecilla, I., Burkhalter, M.D., Popović, M., Fielden, J., Vaz, B., Oehler, J., Pilger, D., Lessel, D., Wiseman, K., et al. (2019). SPRTN protease and checkpoint kinase 1 cross-activation loop safeguards DNA replication. Nat Commun *10*, 3142.

Tang, X., Cao, J., Zhang, L., Huang, Y., Zhang, Q., and Rong, Y.S. (2017). Maternal haploid, a metalloprotease enriched at the largest satellite repeat and essential for genome integrity in Drosophila embryos. Genetics *206*, 1829–1839.

Tateno, H., and Kamiguchi, Y. (2001). Meiotic stage-dependent induction of chromosome aberrations in Chinese hamster primary oocytes exposed to topoisomerase II inhibitor etoposide. Mutat. Res. *476*, 139–148.

Tichy, E.D., Pillai, R., Deng, L., Liang, L., Tischfield, J., Schwemberger, S.J., Babcock, G.F., and Stambrook, P.J. (2010). Mouse embryonic stem cells, but not somatic cells, predominantly use homologous recombination to repair double-strand DNA breaks. Stem Cells Dev. *19*, 1699–1711.

Timmons, L., Court, D.L., and Fire, A. (2001). Ingestion of bacterially expressed dsRNAs can produce specific and potent genetic interference in Caenorhabditis elegans. Gene *263*, 103–112.

Trapnell, C., Roberts, A., Goff, L., Pertea, G., Kim, D., Kelley, D.R., Pimentel, H., Salzberg, S.L., Rinn, J.L., and Pachter, L. (2012). Differential gene and transcript expression analysis of RNA-seq experiments with TopHat and Cufflinks. Nat. Protoc *7*, 562–578.

Uemura, T., Ohkura, H., Adachi, Y., Morino, K., Shiozaki, K., and Yanagida, M. (1987). DNA topoisomerase II is required for condensation and separation of mitotic chromosomes in S. pombe. Cell *50*, 917–925.

Uemura, T., and Tanagida, M. (1986). Mitotic spindle pulls but fails to separate chromosomes in type II DNA topoisomerase mutants: uncoordinated mitosis. EMBO J *5*, 1003–1010.

van Wolfswinkel, J.C. (2014). Piwi and potency: piwi proteins in animal stem cells and regeneration. Integr. Comp. Biol. *54*, 700–713.

Vaz, B., Popovic, M., Newman, J.A., Fielden, J., Aitkenhead, H., Halder, S., Singh, A.N., Vendrell, I., Fischer, R., Torrecilla, I., et al. (2016). Metalloprotease SPRTN/DVC1 orchestrates replication-coupled DNA-protein crosslink repair. Mol. Cell *64*, 704–719.

Voronina, E. (2013). The diverse functions of germline P-granules in Caenorhabditis elegans. Mol. Reprod. Dev. *80*, 624–631.

Wala, J.A., Bandopadhayay, P., Greenwald, N.F., O'Rourke, R., Sharpe, T., Stewart, C., Schumacher, S., Li, Y., Weischenfeldt, J., Yao, X., et al. (2018). SvABA: genome-wide detection of structural variants and indels by local assembly. Genome Res. *28*, 581–591.

Wang, J.C. (1996). DNA topoisomerases. Annu. Rev. Biochem *65*, 635–692.

Wang, J.C. (2002). Cellular roles of DNA topoisomerases: a molecular perspective. Nat. Rev. Mol. Cell Biol. *3*, 430–440.

Ward, W.S., and Coffey, D.S. (1991). DNA packaging and organization in mammalian spermatozoa: comparison with somatic cells. Biol. Reprod. *44*, 569–574.

Woessner, R.D., Mattern, M.R., Mirabelli, C.K., Johnson, R.K., and Drake, F.H. (1991). Proliferation- and cell cycle-dependent differences in expression of the 170 kilodalton and 180 kilodalton forms of topoisomerase II in NIH-3T3 cells. Cell Growth Differ *2*, 209–214.

Wong, M.M., Belew, M.D., Kwieraga, A., Nhan, J.D., and Michael, W.M. (2018). Programmed DNA breaks activate the germline genome in Caenorhabditis elegans. Dev. Cell *46*, 302–315.e5.

Yudkina, A.V., Dvornikova, A.P., and Zharkov, D.O. (2018). Variable termination sites of DNA polymerases encountering a DNA-protein cross-link. PLoS One *13*, e0198480.

Yuen, B.T., Bush, K.M., Barrilleaux, B.L., Cotterman, R., and Knoepfler, P.S. (2014). Histone H3.3 regulates dynamic chromatin states during spermatogenesis. Development *141*, 3483–3494.

Zhang, L., Liang, Z., Hutchinson, J., and Kleckner, N. (2014). Crossover patterning by the beam-film model: analysis and implications. PLoS Genet. *10*, e1004042.

STAR★METHODS

KEY RESOURCES TABLE

REAGENT or RESOURCE	SOURCE	IDENTIFIER
Antibodies		
Rabbit polyclonal anti-PGL-1	Boag Laboratory, Monash University, AU	N/A
Mouse monoclonal anti-PH3	Merck Millipore	06-570; RRID: AB_310177
Mouse monoclonal anti-gamma H2A.X	Abcam	ab26350; RRID: AB_470861
Rabbit polyclonal anti-gamma H2A. X	Abcam	ab11174; RRID: AB_297813
Goat polyclonal anti-ATR	Santa Cruz	sc-1887 (discontinued)
Rabbit polyclonal anti-mouse BRCA1	Namekawa Laboratory, Cincinnati Children's Hospital, USA	N/A
Mouse monoclonal anti-SYCP3	Santa Cruz	sc-74569; RRID: AB_2197353
Mouse monoclonal anti-MLH1	Millipore	NA28; RRID: AB_213130
Mouse monoclonal anti-GFP	Wako	018-20463; RRID: AB_10659145
Rabbit polyclonal anti-GFP	GenScript	A01704; RRID: AB_2622199
Mouse HRP-conjugated monoclonal anti-beta Tubulin	Thermo Fisher Scientific	MA5-16308-HRP; RRID: AB_2537827
Rabbit polyclonal anti-mCherry	Abcam	ab183628; RRID: AB_2650480
Rat IgG Isotype Control	Abcam	ab37361; RRID: AB_2815006
Rat monoclonal anti-TRA98 (GCNA)	Abcam	ab82527; RRID: AB_1659152
Mouse monoclonal anti-PML	Santa Cruz	SC-966; RRID: AB_628162
Bacterial Strains		
E. coli: Strain OP-50	*Caenorhabditis* Genetics Center	WormBase: OP50
E. coli: Strain HT115(DE3)	*Caenorhabditis* Genetics Center	HT115(DE3)
Chemicals, Peptides, and Recombinant Proteins		
1X NuPAGE™ LDS Sample Buffer	Invitrogen	NP0007
DAPI	Abcam	ab228549
Acridine orange	Sigma-Aldrich	65-61-2
Etoposide	Sigma-Aldrich	E1383
Camptothecin	Sigma-Aldrich	C9911
Hydroxyurea	Sigma-Aldrich	H8627
Tetramisole hydrochloride	Sigma-Aldrich	L9756-5G
Tween-20	Fischer	BP337500
NP-40 alternative	Millipore	492018
Protein G Dynabeads	Invitrogen	100004D
Benzonase	Millipore	70746
cOmplete Mini, EDTA-free protease inhibitors	Roche	11836170001
Critical Commercial Assays		
NEBNext® Ultra™ DNA Library Prep Kit for Illumina	New England Biolabs	E7645S
TG NextSeq® 500/550 Mid Output Kit v2 (75 cycles)	Illumina	TG-160-2005
TG NextSeq® 500/550 Mid Output Kit v2 (150 cycles)	Illumina	TG-160-2004
Click-iT EdU Flow Cytometry Assay Kit	Thermo Fisher	#C10424
Deposited Data		
mRNA sequencing of wildtype and Gcna mutant mouse testes at postnatal day 8 (p8) and day 18 (p18). Deposited in the NCBI Sequence Read Archive	this study	BioProject:PRJNA593070
C. elegans genomic DNA sequencing is deposited in the NCBI Sequence Read Archive	this study	SRA:SRP186577; BioProject:PRJNA523775

(*Continued on next page*)

Continued

REAGENT or RESOURCE	SOURCE	IDENTIFIER
Experimental Models: Cell Lines		
Gcna floxed cell line F2E8	Page Lab	N/A
Gcna exon 4 deleted cell line F2E8C3	Page Lab	N/A
Experimental Models: Organisms/Strains		
C. elegans: N2	*Caenorhabditis* Genetics Center	N2
C. elegans: *gcna-1(ne4356)*	Mello Lab	N/A
C. elegans: *gcna-1(ne4444)*	this manuscript	N/A
C. elegans: *gcna-1*(ne4356);*unc-58*(e665)	this manuscript	N/A
C. elegans: *dvc-1(ok260)*	*Caenorhabditis* Genetics Center	RB1401
C. elegans: *dvc-1*(ok260);*unc-58*(e665)	this manuscript	N/A
C. elegans: *dvc-1(ne4442)*	this manuscript	N/A
C. elegans: *dvc-1*(ne4442);*unc-58*(e665)	this manuscript	N/A
C. elegans: *gcna-1*::*GFP*; *top-2*::*mCherry*	Mello Lab	N/A
C. elegans: *gcna-1*::*GFP*; *dvc-1*::*mCherry*	Mello Lab	N/A
C. elegans: *unc-58(e665)*	*Caenorhabditis* Genetics Center	CB665
Mouse: *Gcna* targeted mutation (C57BL/6N-*Gcnatm1.1Dcp*/J)	Jackson Laboratory	RRID:IMSR_JAX:031055
Software and Algorithms		
SEQUEST (version 1.4.0.288)	Thermo Fisher Scientific	RRID:SCR_014594
Scaffold (version Scaffold_4.7.2)	Proteome Software	RRID:SCR_014345
Adobe Photoshop	Adobe	RRID:SCR_014199
Adobe Illustrator	Adobe	RRID:SCR_010279
Graphpad Prism	Graphpad	RRID:SCR_002798
CNVnator v0.3.3	Gerstein Lab	RRID:SCR_010821
FlowJo	Becton Dickinson	RRID:SCR_008520
DNAcopy v1.54	Bioconductor	RRID:SCR_012560
Manta v1.5.0	Chen et al., 2016	https://github.com/Illumina/manta/releases
SvABA v0.2.1	Wala et al., 2018	https://github.com/walaj/svaba
Pixie v0.6	CRUK in house	available on request
Integrative Genomics Viewer (IGV)	Broad Institute	RRID:SCR_011793
Control-FREEC v11.5	Curie Institute	RRID:SCR_010822
VarScan v2.4.3	Washington Univ St. Louis	RRID:SCR_006849
GATK v3.8.0	Broad Institute	RRID:SCR_001876
cuffdiff	University of Washington	RRID:SCR_001647
repBase	Bao et al., 2015	https://www.girinst.org/repbase/
eXpress	Roberts and Pachter, 2013	https://pachterlab.github.io/eXpress/
edgeR	Bioconductor	RRID:SCR_012802
bowtie2	Johns Hopkins	RRID:SCR_005476
Picard v2.18.12	Broad Institute	RRID:SCR_006525
BWA MEM v0.7.17	Li, 2013	http://bio-bwa.sourceforge.net/
fastp v0.19.6	https://github.com/OpenGene/fastp	RRID:SCR_016962

LEAD CONTACT AND MATERIALS AVAILABILITY

Requests for resources and reagents should be directed to and will be fulfilled by Lead Contact, Craig C. Mello (craig.mello@umassmed.edu).

EXPERIMENTAL MODEL AND SUBJECT DETAILS

C. elegans Strains

The N2 Bristol strain of *C. elegans* was cultured at 20°C under standard conditions as described in Brenner (Brenner, 1974) where worms were maintained on NGM media seeded with the OP-50 *E. coli* strain. Deletion alleles of *gcna-1* and *dvc-1* were generated using RNP/*rol-6* strategy, which involves injecting pre-assembled Cas9 ribonucleoprotein complexes and uses *rol-6(su1006)* as the injection marker. Genome editing events between two guides were identified among the F1 rollers (Dokshin et al., 2018). Strains were outcrossed to N2, and balanced with nT1[qIs51] or qC1[qIs26]. The nature of the *gcna-1* alleles (on LGIII) is as follows: *ne4444*: 6006586/6006587-6008976/6008977 (deletion of entire coding sequence with a small insertion inside the breakpoints (AAATTCC TAAAATTTCCTGTATTC)); *ne4356*: 6007278/6007279–6009026/6009027 (1748-bp deletion, removes ATG), described in (Carmell et al., 2016). The *dvc-1(ne4442)* deletion allele on LGV deletes the entire coding sequence: ChrV: 11237535/6-11238944/45. The *dvc-1(ok260)* allele was obtained from the CGC (Strain ID RB1401). The fusion protein lines (*gfp::gcna-1, top-2::mcherry*, and *mcherry::dvc-1*) were described in (Dokshin et al., 2018). All strains are listed in the Key Resources Table.

Bacterial Strains

The OP-50 strain was used for maintenance of worm strains. IPTG-containing RNAi plates were seeded with cultures of HT115(DE3) carrying the appropriate vector (clone V-13G06 and empty vector) for RNAi studies.

Mouse Strains

Gcna-mutant mice (C57BL/6N-*Gcnatm1.1Dcp*/J) are described in (Carmell et al., 2016) and deposited at the Jackson Laboratory. Stock number: 031055. RNA sequencing was carried out from testes of male mice at postnatal days 8 and 18. Immunoprecipitations and spermatocyte spreads were carried out from adult male mice. All mouse studies were performed using a protocol approved by the Committee on Animal Care at the Massachusetts Institute of Technology (Protocol number: 0714-074-17).

METHOD DETAILS

C. elegans Immunohistochemistry and Embryo Analysis

Whole mount preparations of dissected gonads, fixation, and immunostaining procedures were carried out as described in (Dawson et al., 2017). In short, worms were anesthetized and dissected in 0.01% tetramisole and snap frozen on dry ice, then fixed in methanol pre-chilled to -20°C for 20 minutes, then washed twice in PBST for 10 minutes prior to the application of antibodies. Both PGL-1 (gift from Peter Boag) and PH3 (Merck Millipore ab11174) antibodies were used at 1:300 dilutions at room temperature for 2 hours, washed twice in PBST, and secondary antibodies and DAPI (Abcam ab228549) were applied at 1:1000 dilution for 1 hours in darkness prior to mounting and imaging. Live cell imaging of embryos was performed by dissecting young adults on slides in M9 buffer to release early stage embryos. Embryos were collected and immediately mounted on agar pads for imaging.

Topoisomerase Inhibitor, UV, and Drug Treatments

Inhibition of topoisomerase, DNA replication, and inducing dsDNA breaks was achieved by subjecting worms to plates prepared with 70μM etoposide (Sigma-Aldrich E1383), 25mM hydroxyurea (Sigma-Aldrich H8627), and 50μM camptothecin (Sigma-Aldrich C9911) respectively and were performed in triplicates three times as described previously (MacQueen and Villeneuve, 2001). Briefly, twenty L4 staged worms of wild-type and mutant strains were placed on NGM plates enriched with each poison, seeded with OP50 and incubated at 20°C and 25°C for 16 hrs. Worms were then transferred to seeded NGM plates with no poisons for 4 hrs for recovery, then removed. Plates with embryos were then incubated at their respective temperatures for 24 hrs after which time hatching rates were determined.

C. elegans Acridine Orange Staining

Germ cells undergoing apoptosis were assessed *in vivo* via acridine orange as described previously (Boag et al., 2005). Briefly, 20 young adult worms were placed on NGM plates seeded with OP50 and stained with 1ml of 100μM acridine orange (Sigma-Aldrich 65-61-2) for 1 hours, then washed in M9 buffer and immobilized on 2% agarose gel pads in 0.03% tetramisole and observed using DIC and fluorescence microscopy. Each assay was performed at 20°C and 25°C in duplicates and repeated 3 times.

C. elegans Mutator Assay

unc-58(e665) mutator assay was carried out as in (Harris et al., 2006). Briefly, thirty 6cm plates were seeded with OP50 and 5 worms doubly mutant for either *gcna-1* or *dvc-1* and *unc-58(e665)* were added and incubated at 20°C. After several generations, the entirety of each plate of starved worms was chunked onto a large 10cm plate with concentrated OP50 on one side. Plates were scored one week later for revertant worms that were no longer small and paralyzed.

C. elegans Genomic DNA Sequencing

After isolating genomic DNA from worm strains, libraries were prepared using NEBNext® Ultra™ DNA Library Prep Kit for Illumina and sequenced on an Illumina NextSeq machine using a TG NextSeq® 500/550 Mid Output Kits (75 and 150 cycles).

Bioinformatics

Sequence data were demultiplexed and adapter sequences were trimmed from reads using the FASTQ Generation workflow on the Illumina BaseSpace Sequence Hub. Sequence reads were further pre-processed using fastp v0.19.6 (Chen et al., 2018) to trim poly-G tails and aligned to the C. elegans reference genome assembly WBcel235 using BWA MEM v0.7.17 (Li, 2013). Sequence data from 4 lanes of each of 2 runs, one with 37 – 38 nucleotide paired end reads and the other with 150 nucleotide paired end reads, were merged into single BAM files for each sample. Reads were aligned to the *C. elegans* reference genome (ws268; N2 strain) (Table S1). Duplicate read pairs based on aligned positions of each end were marked using Picard v2.18.12 (http://broadinstitute.github.io/picard). Paired sequencing reads were considered to be discordantly mapping with respect to the reference if they fell into one of three categories: 1. Inferred insert size was larger than expected based on the average insert size in the sequencing library, indicating a possible deletion or translocation. 2. Both reads mapped to the same strand, implying the existence of an inversion. 3. Reads mapped to opposite strands but in the wrong orientation relative to the reference, implying the presence of a duplication or translocation. Alignment metrics were computed using Picard CollectAlignmentSummaryMetrics, CollectInsertSizeMetrics and CollectWgsMetrics. Poorly mapped regions for which over 10% of aligned reads are ambiguously placed, multi-mapping reads were determined using the CallableLoci tool from GATK v3.8.0 (McKenna et al., 2010).

Copy number analysis was carried out using VarScan v2.4.3 (Koboldt et al., 2012), CNVnator v0.3.3 (Abyzov et al., 2011) and Control-FREEC v11.5 (Boeva et al., 2012) using the unc-58 sample as a control (note there was a lower mapping rate and hence lower sequencing depth in the N2 control due to likely bacterial contamination). Circular binary segmentation was performed on the relative copy number computed by VarScan using DNAcopy v1.54 (Olshen et al., 2004). Homozygous deletions called by VarScan were assessed using the Integrative Genomics Viewer (IGV) (Robinson et al., 2011).

Genomic rearrangements in each of the 6 mutant samples that are not present in either of the parental strains (N2 and unc-58) were identified using three structural variant callers: Manta v1.5.0 (Chen et al., 2016), SvABA v0.2.1 (Wala et al., 2018) and Pixie v0.6, an in-house discordant read pair and split read clustering tool. Consensus structural variant calls made by and passing filters applied by at least 2 of the 3 callers were assessed using IGV. SvABA filters were as follows: COMPETEDISC: Discordant cluster found with nearly the same breakpoints but differing strands. LOWAS: Alignment score of one end is less than 80% of the contig length or the number of mismatch bases on one end >= 10. LOWMAPQDISC: Both clusters of reads failed to achieve a mean mapping quality > 30. NODISC: Rearrangement was not detected independently of assembly. WEAKDISC: Fewer than 7 supporting discordant reads and no assembly support. Pixie filters: SupportInControl: Fraction of total supporting read pairs from control samples > 0.05. Manta filters: MinSomaticScore: Somatic score < 30.

C. elegans Mortal Germline Assay

Mortal germline assays were performed at 25°C where 10 Individual L1 wild-type and *gcna-1* mutants were placed on individual seeded agar plates until they laid progeny. One worm from the progeny of each plate were transferred to new plates and allowed to mature. This process was repeated until worms were sterile. Brood size and rates of embryonic lethality were recorded on each generation.

C. elegans Co-immunoprecipitation

Frozen pellets of 100,000 synchronized gravid adults were broken by bead beating using a FastPrep-24 benchtop homogenizer (MP Biomedicals) in an equal volume of 1.5× lysis/IP buffer (1× buffer= 250 mM Tris HCl pH 7.5, 150mM Sodium Chloride, 50mM Sodium Citrate, 1mM DTT) supplemented with cOmplete Mini, EDTA-free protease inhibitors (Roche 11836170001). The lysate volume was adjusted to 1ml with 1× lysis buffer and sonicated on medium for 3 minutes (15 seconds on 60 seconds off) followed 45 seconds on high (15 seconds on 60 seconds off) in a Bioruptor (Diagenode). Lysate was then supplemented with 1% NP-40 alternative (Millipore 492018) and incubated rotating for 1 hours at 4°C. Carcasses were spun down and supernatant was pre-cleared with 100μL pre-washed Protein G Dynabeads (Invitrogen 100004D) rotating at 4°C for 1 hours. Immunoprecipitations were carried out at 4°C overnight with mouse anti-GFP monoclonal antibody (Wako 018-20463). Antibody was captured with 100μl pre-washed Protein G Dynabeads at 4°C for 2 hours, and washed 3× with IP buffer. Protein was eluted for 10 minutes at 70°C in 150 μl of 1× NuPAGE™ LDS Sample Buffer (Invitrogen NP0007) with 100mM DTT and 20μl of the elution was used for a western blot. For input, 4μl of input (0.4% of starting material) was used to detect TOP-2. GCNA-1 was not detectable in input even in 4% of the starting material. Western blotting was performed with rabbit anti-mCherry polyclonal antibody (Abcam ab183628; 1:1000), rabbit anti-GFP (Genscript; 1:1000), and Tubulin-HRP (Thermo Fisher; 1:1000).

C. elegans RNAi

chk-1 RNAi was done by feeding with clone V-13G06 and empty vector from the Ahringer RNAi Library (Source Bioscience) (Timmons et al., 2001). The N2 strain was used as wild type in all experiments. IPTG-containing RNAi plates were seeded with cultures of HT115(DE3) carrying the appropriate vector. For RNAi treatment, L4 larvae were placed on RNAi plates for 20 hours at 20°C, and single picked onto blank plates for egg laying. Immediately after removal of the adult worm, embryos were counted and scored for hatching 24 hours later.

C. elegans Brood Counts

Brood and male frequency counts were performed at 20 and 25°C. Briefly, animals were single picked at mid-L4 stage and followed with daily transfers until they produced no more progeny. Animals were counted when the population on a progeny plate reached adulthood.

Mouse Testis Histology

Mouse testes were fixed overnight in Bouin's fixative at 4°C, then transferred to 70% ethanol before processing and embedding in paraffin. Five-micron sections were stained with hematoxylin and eosin before histological examination.

Mouse ES Cell Flow Cytometry

Mouse ES cells were grown in ES cell media (high glucose DMEM, 10% FCS, glutamine, 1mM sodium pyruvate, non-essential amino acids, 0.1mM 2-mercaptoethanol, penicillin, streptomycin, 10^3 units/ml LIF) on a layer of inactivated feeder cells. To discriminate the cell cycle, cells were cultured in 20μM EdU (AbCam #146186) for 10 min. A single cell population was isolated by trypsinization, and blocked in 10% FCS. Cells were fixed in 4% PFA for 15 minutes, and permeabilized in 0.5% Triton X-100 for 15 minutes, and re-suspended in 1% bovine serum albumin (Sigma #A2153). Cells were then stained with an antibody to Tra98 (Abcam#82527; 1:100), detected with a secondary fluorophore (Jackson Immuno #712-096-150). Gates were set using both a no-antibody control, and *Gcna*-mutant ES cells were stained in parallel to establish a threshold for GCNA expression over background. Edu was detected with Click-iT EdU flow cytometry assay kit (ThermoFisher #C10424) according to the manufacturer's instructions, with DNA labeled with DAPI. Cell cycle and Tra98 staining was detected using a FACS Aria II sorter (BD Biosciences) using BD FACSDiva Software Version 8.0 and FlowJo Software Version 10.5.3.

Calculation of Crossover Interference

To estimate the strength of crossover interference, we fit a gamma distribution to the distances between MLH1 foci on chromosomes with more than one focus, following the method of (de Boer et al., 2006). Briefly, we binned inter-crossover distances by chromosome length, and fit the observed distribution of inter-crossover distances to a gamma distribution using Scipy, obtaining initial estimates of the gamma shape and scale parameters. Then, we refined our shape and scale estimates, used a simulation approach to correct for the fact that interfocus distances cannot be greater than chromosome length or shorter than the resolution of our immunofluorescence images.

RNA Sequencing

Total RNA was isolated from the testes of 2 wild-type and 2 *Gcna*-mutant mice using Trizol at both postnatal day 8 and postnatal day 18. RNA was enriched for polyA and sequencing libraries were prepared by the Whitehead Institute Genome Core Facility and sequenced on an Illumina HiSeq with 75-bp paired end reads. For genome-wide differential expression analysis, reads were aligned to the mouse genome (mm10) using TopHat and fold-changes and p-values were calculated using cuffdiff (Trapnell et al., 2012). For analysis of transposon expression, LTR and non-LTR retrotransposon sequences were downloaded from repBase (Bao et al., 2015), reads were aligned to the retrotransposon sequences with bowtie2 (Langmead et al., 2009), expression of each transposon was quantified with eXpress (Roberts and Pachter, 2013), and differential expression analysis was performed with edgeR (Robinson et al., 2010).

Mouse Spermatocyte Spreads

Mouse spermatocyte spreads were carried out as in (Peters et al., 1997). Briefly, meiotic cells were isolated from mascerated seminiferous tubules, spun down and resuspended in hypotonic buffer (30 mM Tris-HCl pH 8.2, 50 mM sucrose pH 8.2, 17 mM sodium citrate). After a second spin they were resuspended in 0.1 M sucrose and dropped onto the slides wet with 1% PFA, 0.1% Triton X-100 in sodium borate buffer pH 9.2 and incubated in a humid chamber for 2–3 hr. For immunostaining, slides were blocked in 3% BSA and incubated with primary and secondary antibodies in 1% BSA. Nuclei were stained using the following antibodies: mouse anti-H2A.X phosphorylated on Ser 139 (anti-γH2A.X) (Abcam ab26350; 1:1000), rabbit anti-γH2A.X (Abcam ab11174; 1:1000), goat anti-ATR (Santa Cruz sc-1887; 1:100), rabbit anti-mouse BRCA1 (gift of S. Namekawa, 1:500), mouse anti-SYCP3 (Santa Cruz sc-74569; 1:100), mouse anti-MLH1 (Millipore NA28; 1:100).

Embryonic Stem Cell Survival Assay

ES cells were cultured under standard conditions. Cells were trypsinized, counted, and 500 cells were plated at clonal density in triplicate for each condition. After cells had adhered to the plate, media was removed and cells were irradiated with indicated doses of UV using a Stratalinker. 7–10 days later, surviving colonies were stained with Crystal violet and counted.

Immunoprecipitation from Mouse ES Cells

Mouse ES cells were irradiated with 8J/m2 UV, harvested 1 hours later by scraping, and suspended in IP buffer: 50 mM HEPES pH 7.4, 140 mM NaCl, 10% glycerol, 0.5% NP-40, 0.25% Triton, 100 μM ZnCl2 plus cOmplete Mini, EDTA-free Protease Inhibitor Tabs (Roche 11836170001). Samples were sonicated on ice 1 min at 30% amplitude using a Branson Sonifier and treated with 100 U/ml

Benzonase (Millipore 70746) for 20 min on a rocker at room temperature. Samples were spun down for 10 min at 16,000 G at 4°C, and supernatant was used for immunoprecipitations. After extensive washing in IP buffer, precipitated proteins were subjected to SDS–PAGE and silver staining.

Mass Spectrometry

Samples were processed at the Whitehead Institute Proteomics Core Facility. For mass spectrometry analysis, bands were excised from each lane of a gel encompassing the entire molecular weight range. Trypsin digested samples were analyzed by reversed phase HPLC and a ThermoFisher LTQ linear ion trap mass spectrometer. Peptides were identified from the MS data using SEQUEST (RRID:SCR_014594). Sequest searched refseq_mouse_6mich_122812.fasta (refseq_mouse plus the unannotated GCNA sequence, 26784 entries) assuming the digestion enzyme trypsin with a fragment ion mass tolerance of 0.80 Da and a parent ion tolerance of 10.0 PPM. Carbamidomethyl of cysteine was specified as a fixed modification. Methyl of arginine, oxidation of methionine and dimethyl of arginine were specified in Sequest as variable modifications. Scaffold (version Scaffold_4.7.2, Proteome Software Inc.) was used to validate MS/MS based peptide and protein identifications. Peptide identifications were accepted if they could be established at greater than 95.0% probability by the Scaffold Local FDR algorithm. Protein identifications were accepted if they could be established at greater than 99.0% probability and contained at least 2 identified peptides. Protein probabilities were assigned by the Protein Prophet algorithm within Scaffold. Proteins that contained similar peptides and could not be differentiated based on MS/MS analysis alone were grouped to satisfy the principles of parsimony. Proteins sharing significant peptide evidence were grouped into clusters.

Microscopy

Immunohistochemistry and acridine orange staining were imaged on a Zeiss Axio Imager M2 and captured using an Axiocam 506 mono camera (Zeiss). Figures were constructed using Photoshop and Illustrator (Adobe) and graphs and statistical analysis was performed using Graphpad Prism (Graphpad). Mouse spermatocyte spreads were imaged using a DeltaVision system (Applied Precision) and subjected to deconvolution and projection using the SoftWoRx 3.3.6 software (Applied Precision). Live cell imaging of *C. elegans* embryos was carried out using a Zeiss Axio Imager M2 (Zeiss) with images collected every 15 to 30 seconds using an ORCA-Flash 4.0 digital camera (Hamamatsu) and processed using Zen software (Zeiss). Brightness in some panels of Figure 5B was increased relative to earlier images in the time course to compensate for bleaching of the fluorescent signal over time, but does not affect the interpretation of this qualitative data.

QUANTIFICATION AND STATISTICAL ANALYSIS

Quantification and statistical analysis was performed using Graphpad Prism (Graphpad). Statistical parameters, numbers of animals and repetitions for each experiment are listed in their associated figure descriptions.

DATA AND CODE AVAILABILITY

The *C. elegans* genomic DNA sequencing data reported in this paper is publicly available from NCBI's Sequence Read Archive under the accession: SRA:SRP186577 BioProject:PRJNA523775. mRNA sequencing of wildtype and Gcna mutant mouse testes at postnatal day 8 (p8) and day 18 (p18) is also deposited in the NCBI Sequence Read Archive under the accession BioProject: PRJNA593070. An in-house script (Pixie v0.6) was used for discordant read analysis and is available upon request.